

Optical gain and photo-bleaching of organic dyes, quantum dots, perovskite nanoplatelets and nanodiamonds

Mahendran Vellaichamy¹, Miha Škarabot^{1,2}, and Igor Muševič^{1,2*}

¹Condensed Matter Department, J. Stefan Institute, Jamova 39, SI-1000 Ljubljana, Slovenia

²Faculty of Mathematics and Physics, University of Ljubljana, Jadranska 19, SI-1000 Ljubljana, Slovenia

*Corresponding author: igor.musevic@ijs.si

Abstract

Optical gain and resistance against photo-bleaching are key material parameters for practical applications in microlasers and microphotonics. Here we present studies of optical amplification and photo-bleaching in a wide range of optical gain materials, including fluorescent dyes, quantum dots and rods, organic and inorganic room temperature polaritons, and nanodiamonds with emission range from 430 - 680 nm. We used amplified spontaneous emission (ASE) for each material to measure the optical gain. Robustness against photo-bleaching was determined by measuring the intensity of spontaneous emission of the material as a function of the number of excitation femtosecond pulses (10^6 - 10^{10}) at various excitation energy densities. We show that pyrromethene laser dyes are the best organic emitters in terms of low excitation energy and good optical gain, whereas solid-state polariton materials are better in terms of high optical gain and stability. We find that all organic and inorganic optical gain materials bleach completely after 10^6 to 10^9 illumination pulses with typical 0.1 to 0.6 GW/cm² peak power density, with a clear exception of nanodiamonds. We show that nanodiamonds are the only optical gain material that shows no photo-bleaching beyond the 10^{10} excitation pulses of 300 fs pulse duration and with 0.16 GW/cm² peak power density.

Key Words: ASE, VSL method, optical gain, photostability, dyes, polaritons, anthracene, nanodiamonds, microdroplet laser

1. Introduction

In recent years efforts to realize optically pumped low-threshold lasing from the photonic band edge of a laser dye-doped cholesteric liquid crystal (CLC) have been focused on developing new optical gain materials with optimized pumping parameters and enhanced photostability [1–9]. Numerous organic, inorganic, and biological optical gain materials have been explored, but the obtained results are difficult to compare due to the different methods used. There is clearly a need for a characterization method to screen optical gain materials for specific applications in microdroplet liquid crystal lasers [10–13]. In a small, ten micrometer diameter droplet laser, optical gain material is strongly confined and isolated from the external reservoir of gain molecules. Under these circumstances, the fluorescent organic molecules are exposed to intense optical excitation, which gives rise to a rapid bleaching and decrease of lasing intensity. For example, a $\sim 20\text{ }\mu\text{m}$ nematic liquid crystal droplet with fluorescent dye is lasing for only some ten minutes under the repetition rate of $\sim 100\text{ Hz}$ and illumination peak power density of $\sim 10\text{ MW/cm}^2$. The life time of such dye lasers is clearly far from practical use and has to be improved.

The aim of this study is to measure the optical gain and rate of photo-bleaching of a variety of materials that are used, or are considered to be used in liquid crystal microdroplet lasers. Typically, LC microdroplet lasers are droplets of a nematic [14, 15], chiral nematic [16] or even ferroelectric liquid crystals [17] dispersed in another medium that does not mix with that particular LC. For example, nematic droplets of 5CB are dispersed in water with added surfactants to control the surface anchoring, which controls the internal director structure of the droplet [15]. Whispering Gallery Mode (WGM) lasing is obtained from such a droplet, if optical gain is added to the LC, and is excited by external light pulses. The optical gain material is usually fluorescent organic dye that easily dissolves in LC and has large quantum yield. The excitation of electronic transitions within gain fluorescent molecules will give rise to spontaneous and stimulated emission of light. Because a LC droplet is an optical cavity that sustains WGMs, lasing will take place from these modes, generating characteristic WGM spectrum of sharp lines [14,15]. In a WGM microlaser, made of nematic droplet with dissolved fluorescent dye, the typical lasing threshold fluences of the excitation (pump) pulsed beam is of the order of $\sim 1\text{ mJ/cm}^2$ and typical pulse duration is $\sim 1\text{ ns}$.

It has been shown, that such WGM laser can be controlled by low external electric field over significant range of emitted wavelengths. Similarly, omnidirectional lasing is obtained from cholesteric droplet with onion-like director structure [16]. In reality, the life time of such micro-lasers based on fluorescent organic dyes is some ten

minutes, and the lasing intensity decreases due to the photo-induced bleaching of fluorescent dyes. This is a very old and well-known problem of dye lasers, which becomes quite severe, if the laser is small and the bleached fluorescent material cannot be replaced like, for example, by circulating the dye solution through the cavity of dye laser or by natural diffusion. It is therefore of vital importance to design an optical gain material that can: (i) dissolve well in liquid crystals, (ii) has high optical gain and (iii) does not bleach under realistic number of excitation cycles, which is typically $>10^{12}$.

The optical gain of a particular material is conveniently measured using the Amplified Spontaneous Emission (ASE) [18,19]. In a typical ASE experiment the illuminating light is shaped into a thin stripe of variable length, hence the method is known as the variable stripe length method (VSL). The stripe of light is illuminating the optical gain material that is usually deposited in a form of a thin layer on a substrate, and the excitation light is usually absorbed in a few micrometer thin surface layer. The fluorescent light that emerges from the edge of the illuminated stripe is measured as a function of the stripe illumination intensity and length. The photo-stability, i.e. resistance against photo-bleaching, is yet another vital parameter to characterize the optical gain medium, which is the measure of given optical gain material/fluorophore to withstand cycles of emission (bright excited state) and absorption (dark ground state) without irreversible damage.

The aim of this article is two-fold: (i) First, we want to measure and compare the magnitude of optical gain coefficient in different materials, but keeping the method, the setup and the parameters of the measurement equal for all the materials under study. (ii) Second, we want to determine the emitted fluorescent intensity as a function of the number of excitation pulses for all materials under study, keeping the method, the setup and the experimental parameters equal for all the materials studied. It is not our aim to explore or comment on the mechanism of photo-bleaching, as this has been extensively discussed in the literature over the past 50 years. It is also not our aim to study lasing using these materials, as this is the aim of ongoing studies that will be published in near future.

In this article we present optical gain measurements from: (i) different fluorescent dyes, dissolved in planar aligned 5CB liquid crystal, (ii) quantum rods (QRs) and quantum dots (QDs) deposited on glass, (iii) perovskite nanoparticles deposited on glass, (iv) fluorescent silica nanobeads deposited on glass, (v) anthracene nanoplatelets in different solvents or organic matrices and (vi) nitrogen vacancy NV nanodiamonds deposited on glass and NVN nanodiamonds in water dispersion. In addition to the ASE, we perform extensive measurements of photo-bleaching of different organic dyes and compare to bleaching of organic and inorganic polariton materials and nanodiamonds. We conclude that room temperature inorganic polaritons are superior in terms of photo-stability and optical gain, which is much lower for fluorescent dyes. Finally, we find that nanodiamonds are far superior in terms of

practically negligible photo-bleaching beyond the 10^{10} illumination pulses, while demonstrating modest optical gain.

2. Materials and Sample preparation

2.1. Laser dyes

Laser dyes have traditionally been used as high optical gain material with good and selective solubility in different solvents and extremely high brightness. While direct use of organic dyes in high power tuneable dye lasers has been abandoned, they are heavily used in fluorescent imaging. Their main disadvantage is high susceptibility to photo-bleaching, thereby fluorescent intensity compensation due to bleaching has to be considered during imaging. For this study we have chosen laser dyes Pyrromethene 567, Pyrromethene 580, Pyrromethene 597, Pyrromethene 650, 4(Dicyanomethylene)-2-methyl-6-(4-dimethylaminostyryl)-4H-pyran (DCM) and Nile Red (NR), with some properties listed in Table 1. Nematic liquid crystal 4-Cyano-4'-pentylbiphenyl (5CB, Nematel GmbH & Co. KG, Mainz) is used as a host, and organic dyes are readily dissolved in a typical nematic liquid crystal host up to ~ 2 wt%. We have chosen rather low mass concentration of dyes in 5CB, typically ~0.25wt%. Dyes were dissolved directly in the isotropic phase of the nematic LC at the temperature of 50°C for 15 minutes, while mixing with mechanical vortex shaker and by applying intense ultrasound. The LC-dye dispersion was centrifuged before the experiment to sediment the undissolved dye crystals, and care was taken not to introduce dye particles into the LC cells. LC-dye mixture was filled in the planar cell used in all the experiments. The cells were made of two 0.7 mm glass slides coated with polyimide SE-5291 (Nissan Chemical) and unidirectionally rubbed to obtain good planar alignment of 5CB. The thickness of all LC cells was kept constant at 19 ± 1 μm for all ASE a photo-stability experiments.

Table 1. Summary of the fluorescent properties of organic dyes used in this study.

Parameter	PM 567	PM 580	PM 597	PM650	DCM	NR
Fluorescence life time	213 ns	218 ns	203 ns	220 ns	2 ns	2.8 ns
Quantum yield	0.99 (in Methanol)	0.90 (in Ethanol)	0.77(in Ethanol)	0.54 (in Methanol)	0.43 (in Methanol)	0.7 (in Dioxane)
Absorption peak max	532 nm (Ethanol)	532 nm (Ethanol)	532 nm (Ethanol)	588 nm (Ethanol)	532 nm (Ethanol)	530 nm (Methanol)

Emission peak max	567 (Ethanol)	547-581 (Ethanol)	566-611 (Ethanol)	604-630 (Ethanol)	594-630 (Ethanol)	630-640 (Methanol)
----------------------	------------------	----------------------	----------------------	----------------------	----------------------	-----------------------

2.2 Room temperature exciton-polariton semiconductor nano-crystals, quantum dots, fluorescent beads and nanodiamonds

While fluorescent organic dyes are readily dissolved in nematic LCs, the problem of dispersing tens of nanometer-size particles in nematic LCs is much more complex due to the aggregation of particles. Namely, any colloidal inclusion larger than some tens of nanometers that is placed in a nematic liquid crystal, exhibits long range attractive forces to neighbouring particles due to the elastic distortion of the LC around each inclusion. This results in strong and rather fast aggregation of dispersed particles, leading to formation of clusters. For example, it has been shown that even 22 nm silica particles dispersed in 5CB get aggregated after some time and the growth of aggregates is self-amplified as the clusters grow [20–22]. It is therefore expected that aggregation of nanocrystals, quantum rods and dots dispersed in a nematic LC is a serious problem in nematic. It has been shown that in some cases this aggregation can be prohibited by adding gelators to the LC thus forming a nematic gel [23]. To avoid problems with fluorescent particles aggregation in 5CB, we measured optical gain of a thin layer of solid particles deposited from solution on glass.

Exciton-polariton materials exhibit hybridization of excitons with confined light modes [24] and are promising for the realization of low threshold lasing due to their high-optical gain reported in the literature [25]. While organic semiconductors sustain polaritons at room temperature and have been extensively studied for room temperature polariton devices, there is little information on their performance in terms of photo-bleaching. In our studies we were using organic semiconductor Anthracene (Sigma-Aldrich), and organic semiconductor perovskite CsPbBr₃ and CsPbI₃ nanoparticles (Mesolight). In addition to organic exciton-polariton materials, we studied fluorescent silica nanobeads (hiQ nano) as inorganic polariton materials. We also measured optical gain and photo-bleaching on thin layers of inorganic semiconductor CdSe/CdS quantum rods (Sigma-Aldrich), CdSe/ZnS quantum dots (Sigma-Aldrich), Fluorescent NV nanodiamonds (Nitrogen vacancy >900 NV/particle, Sigma-Aldrich) and green fluorescent NVN nanodiamonds (Adámas Nano). Some of the material properties are summarized in Table 2. A known concentration of particles is dispersed in organic solvent (hexane/toluene/methanol). To ensure homogenous distribution of particles, each dispersion was ultrasonicated for 5 minutes. Thin films of dispersed materials are prepared by drop casting 20-30µl of dispersions on glass surface to get nearly uniform dry film. In all cases, except for the NV nanodiamonds, the deposited and dried film showed characteristics of a crystalline

layer, indicated by regular and straight defect lines across the film. Particle size and particle concentration are given in Table 2. NVN nanodiamonds were studied in water dispersion that was introduced in a 7 μm thick glass cell.

Table 2. Summary of fluorescent properties of solid-state nanoparticles and nanocrystals used in this study. The particle composition, size, concentration, surface functional group and quantum yield were provided by supplier.

Material		λ_{ex} (nm)	λ_{em} (nm)	Size (nm)	Concentration	Quantum yield	Surface functionality	Supplier
Quantum dots/rods	CdSe/CdS	532	560	5×30	0.5 wt% in hexane	> 0.70	octadecylamine ligands	Sigma- Aldrich
	CdSe/ZnS	532	566	6.8	0.5 wt% in toluene	> 0.50	octadecylamine ligands	Sigma- Aldrich
Perovskites	CsPbBr ₃	450	514	18	3 wt% in toluene	0.90	organic	Mesolight LCC
	CsPbI ₃	450	684	38	3 wt% in toluene	0.78	organic	Mesolight LCC
	CsPb (Br ₃ /I ₃)	450	631	40	3 wt% in toluene	0.80	organic	Mesolight LCC
Organic polaritons	Anthracene	400	423		2 wt% in toluene	n.a.	n.a.	Sigma- Aldrich
Fluorescence nanobeads	Silica	570	590	25	1 wt% in water	n.a.	Carboxylic acid	Hiq-nano
NV Nanodiamonds	NV>900 / particle	532	645	100	0.2 wt% in acetone	n.a.	Amine	Sigma- Aldrich
NVN nanodiamonds	synthetic type Ib diamond	488	513	120	0.1 wt% in water	n.a.	Carboxylic acid	Adámas Nano

3. EXPERIMENTAL

3.1. Methodology

Optical gain coefficient (g) quantifies the amount of light, amplified per unit length, as it propagates through excited gain medium. ASE emission from different dyes in planar aligned nematic LC host 5CB is measured by the Variable Stripe Length method (VSL) [19,26,27]. This method involves the detection of single-pass amplified

light, emitted along the thin slab of an optically excited matter and was developed by Shaklee and Leheny in 1971 [19]. In the VSL method a stripe-shaped beam is illuminating the surface of optical gain material, such as a crystal surface or a cell filled with solution of fluorescent dyes. The depth of the excited region is usually quite small, i.e. of the order of few micrometers. Spontaneous fluorescence is amplified by stimulated emission, as the emitted light passes through the excited volume to the edge of the optical gain material. The stripe therefore acts as an optically pumped waveguide. If the spontaneous emission is isotropic and uniform in the excited volume, the intensity of the amplified light in the small gain model [18], exiting from the edge of the illuminated stripe is:

$$I_{ASE} = \frac{AI_s}{g}(e^{gL} - 1) \quad (1)$$

Here A is the cross-sectional area of the excited volume, I_s is the spontaneous emission rate per unit volume and g is the net gain experienced by light, $g = g' - \alpha$, where g' is the gain due to stimulated emission and α is the optical loss. L denotes the stripe length. From the ASE intensity as a function of stripe length at constant surface energy density (fluence) of the excited light, the optical gain can be determined [19]. The stimulated emission is detected from the nearly exponential increase in the detected intensity, when the length of the excited stripe is increased. This is most easily seen in log-lin plot of I_{ASE} as a function of L , where the slope of the linear part of the curve indicates the optical gain parameter g , see Fig. 2 in Ref. 15. It is also clear that by increasing the surface energy density of the excitation light, the optical gain parameter increases. It is therefore of vital importance to keep all experimental parameters (such as the fluence of excitation light) constant, when comparing optical gain of different materials in different experiments.

The choice of stripe length is very important in the VSL method, and, based on the literature data [26], we chose 1.4 mm as the maximum stripe length. Apart from the dependence on stripe length, the ASE-VSL measurements were carried out with different stripe beam polarization, and pump power density. Polarization of the excitation beam is important for the ASE experiments on fluorescent dyes dissolved in nematic liquid crystals. It is well known that the majority of dye molecules align their radiating dipoles with respect to the local direction of LC molecules. Most of dyes align their radiative dipoles along the direction of LC alignment, also called the director. There are some exceptions, which align their radiative dipoles perpendicular to the director. Polarization of the excitation light should not be relevant for effectively spherical particles, while it could be relevant for Quantum Rods (QRs) due to their elongated shape.

3.2. Experimental set-up

The ASE measurement setup that we used in our experiments is schematically shown in Figure 1. The setup uses a tuneable 300 femtosecond laser ORIGAMI XP (NKT Photonics) that can be tuned in the UV, visible and IR, and provides variable repetition rates from single shot up to 100 kHz to illuminate the optical gain material. The laser beam was first expanded using a combination of a plano-concave lens L1 and double convex lens L2 to get a 5 mm diameter Gaussian beam. A cylindrical lens L3 with a focal length of 150 mm is used to create a thin stripe of light in the focal plane of this lens, i.e. along the cylindrical axis. The direction of the light stripe is horizontal, i.e. parallel to the surface of the optical table, where the experiments have been performed. The divergence of this strip of light is several degrees. A fixed slit FS of dimensions 2×15 mm was placed in the focal point of lens L3 to create a fixed stripe of light with length of 10 mm. This fixed slit was used to select the nearly uniform intensity region of the stripe from the Gaussian profile of the incident beam. A variable slit AS, mounted on a precision linear stage was placed at a separation of ~ 3 mm from the FS to control the strip length in horizontal direction. The length of this stripe could be controlled with a precision of $5 \mu\text{m}$. A combination of convex lenses L4 and L5 were put at a distance of 195 mm from FS to minimize the diffraction effects from the slits. This set of lenses produced an image of the light strip on the surface of the measuring sample. The dimensions of this light stripe were 1.4 mm (maximum length) \times 0.1 mm (constant width). In this way the thin stripe of light illuminates the sample and excited the fluorescence. The stripe was set horizontally (parallel to the optical table) and the plane of polarization of the illuminating stripe was changed either parallel or perpendicular to the stripe using a half-wave plate HWP polarization rotator. Another polarizer P was used to precisely define the plane of polarization. A combination of two convex lenses was used to focus the fluorescent emitted light, emitted from the edge of the sample, into the tip of the collecting fiber (step-index multimode, with $105 \mu\text{m}$ silica core, 0.22 NA, wavelength range 400 – 2400 nm (Low OH)). A green filter F1 (notch filter, 532 nm) was used to remove the signal of the excitation beam, which was reflected from the glass edges of the LC cell. In the experiment, ASE light was collected from the edge of the fluorescent layer, i.e. the axis of the collecting optics was parallel to the illuminated stripe of fluorescent molecules. The ASE signal was coupled to CCD imaging spectrophotometer (Andor, Newton EMCCD, Czerny-Turner spectrograph) through a multimode fibre optic cable (step-index multimode, with 105-micron silica core, 0.22 NA, wavelength range 400 – 2400 nm (Low OH)).

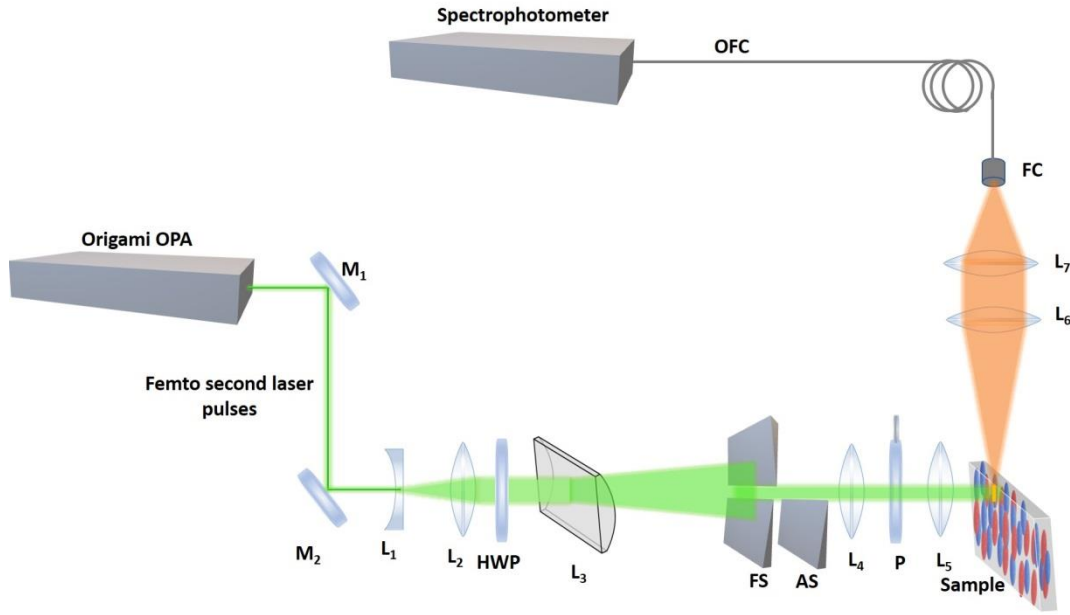


Figure 1. Schematic diagram of the experimental setup for ASE orientation measurements. The plane of polarization is rotated with a half-wave plate (HWP). M1, M2 dielectric mirrors, L1-L7 lenses, HWP – halfwave plate (@532nm), P-polarizer, FS-fixed slit, AS- Adjustable slit, FC- fibre coupler.

Figure 2(a) shows images of the fluorescent stripe with a variable length. For maximum length of 1.4 mm, the illuminated surface area on the sample is $\sim 0.0014 \text{ cm}^2$. For a typical pulse energy of $\sim 1 \mu\text{J}$, the surface energy density at the sample is $\sim 710 \mu\text{Jcm}^{-2}$. Single pulse duration of Origami OPA is 300 fs, which gives peak power density of $\sim 2.4 \text{ GW/cm}^2$ during $\sim 1 \mu\text{J}$ pulse illumination. The light is collected from the left-hand side edge of the stripe. Figure 2(b) shows the spectra of collected ASE light from the $\sim 3 \mu\text{m}$ thick film of 5CB mixed with Nile red.

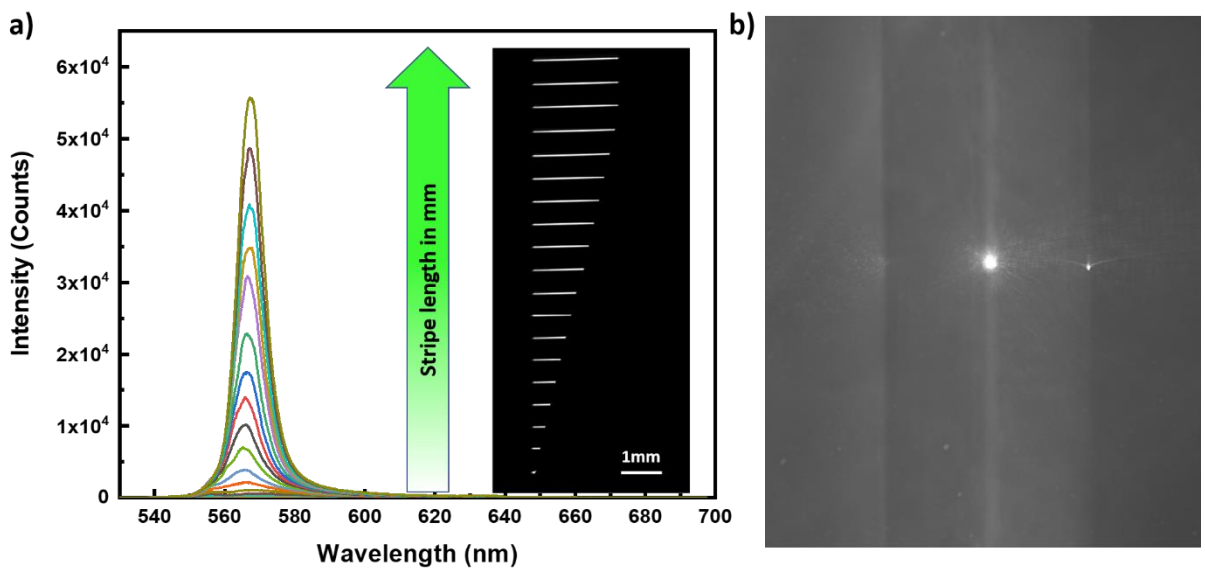


Figure 2: Typical ASE measurement. (a) The ASE intensity is measured for Pyrromethene 567, dissolved in 5CB at different stripe lengths of the excitation beam. The width of the stripe is $50\pm 5\mu\text{m}$. On the left are the ASE spectra, collected from the edge of the LC cell for different stripe lengths. On the right is monochrome image of increasing stripe length. (b) Side-view of the ASE light emitted from the side of the sample. The bright spot in the centre is the ASE light exiting the illuminated stripe. On the left and right of this bright spot there are two glass slides (vertical on this picture) of thickness $700\mu\text{m}$, placed parallel at a separation of $20\mu\text{m}$. This gap between the two plates is filled with LC and fluorescent dye and appears slightly brighter than glass plates.

4. Results and Discussion

4.1. Optical gain

4.1.1 Optical gain of organic fluorescent dyes in a LC

The polyimide rubbing on the surfaces of the measuring cells gives unidirectional planar orientation of the nematic 5CB liquid crystal. All the dye molecules used in the work are rod-like, so they are expected to align along the nematic director. This means that dye molecules are most strongly excited, if the polarization of the excitation light is perpendicular to the rubbing direction, i.e. parallel to the radiative electric dipole. The emission from the transition dipole of the dye molecule is expected to be maximal in a perpendicular direction to the radiative dipole and is therefore spatially anisotropic due to the alignment of dye molecules along the LC director.

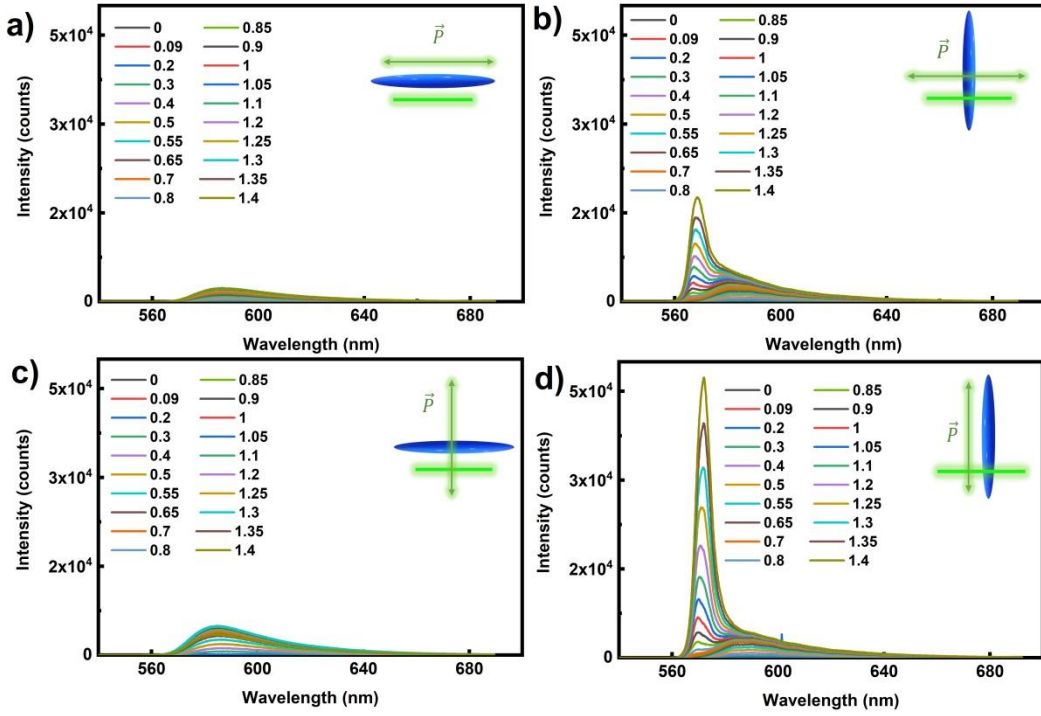


Figure 3. (a-d) The orientation dependence of ASE emission spectra from 5CB+ PM 580 dye for different stripe length in a 19 μm thick planar cell. Here the green line represents the stripe beam, the green arrow represents the direction of polarization and the blue ellipsoid represents the LC orientation (director of LC or the rubbing direction). The excitation wavelength is 532 nm, 300 fs pulse with energy of 30 μJ per pulse and the ASE light is collected from 40 pulses at a repetition rate of 10 Hz. The different colour spectrum corresponds to different stripe lengths from 0 – 2 mm, as shown in the legends for each panel.

We first investigate the emission intensity for various pump beam polarization with respect to the orientation of LC director (and dyes). As shown in the insets to Fig.3, four different orientations of director and pump polarization with respect to the light stripe are used: (a) the director and direction of polarization are parallel to stripe, (b) the director is perpendicular to the stripe and polarization (c) the polarization of light is perpendicular to the director and light stripe, and (d) both the director and the direction of polarization are perpendicular to the light stripe.

Figure 3 shows the polarization-dependent ASE spectra for two different orientations of PM580 with respect to the light stripe direction (parallel and perpendicular). As evident from Figure 3, for the three orientations in panels (a-c), the ASE intensities are quite low, and the emission spectra appear quite broad. When the pump beam polarization is parallel to the director and both are perpendicular to the stripe, a strong ASE peak appears, as shown in Fig. 3d. By increasing the stripe length (shown by different colours), the emission peak narrows, which is a

clear indication of enhanced optical amplification by stimulated emission. Namely, the optical gain depends on the wavelength, $g(\lambda)$, and by increasing amplification, certain wavelengths are strongly amplified, which results in narrowing of the emitted ASE spectrum. It is interesting to note that in addition to a single and broad ASE peak at small stripe lengths, another ASE peak emerges at intermediate stripe lengths and becomes dominant at large stripe lengths, see Figure 3d. To clarify this, we performed similar ASE experiments on 0.25 wt% PM 580 dissolved in index matching microscope oil. The ASE spectrum of PM 580 in the isotropic oil shows only a single and rather broad fluorescent peak. This could be explained by considering orientational ordering of dye molecules in the NLC. Whereas in a NLC, the PM 580 molecules are obviously ordered along the director, they are completely orientationally disordered in an isotropic oil. This clearly points out that the two ASE peaks are due to orientational order of PM 580 molecules in a NLC. We conjecture that the PM 580 molecules have two radiative moments or two excited states that have different optical gain and different emission wavelengths. In an isotropic oil, the emitted spectra is time and space-averaged, which results in a single and broad fluorescent emission peak. In 5CB, the two emitters of an aligned PM 580 molecule give two different optical amplification factors, depending on the quantum mechanical properties of electron orbitals of the PM 580 molecule.

A similar response is obtained for PM 567, PM 597, PM 650, DCM, and Nile Red dissolved in 5CB. The strong ASE emission for pump beam polarization along the director can be understood in terms of the transition dipole moment direction of dyes. The emission of light is highest in the plane, perpendicular to the emitting dipoles; hence we obtain maximum light amplification, when this emitted light travels along the stripe and amplifies itself. However, there is one exception, as the isomeric dye pyrromethene 597 shows different polarization dependence on ASE emission [28]. Strong ASE is obtained nearly for all polarizations and director orientation with respect to the stripe. This can be attributed to the nearly symmetric molecular structure of this dye, and, for a given polarization direction, some of the dipoles are contributing to the ASE signal.

Because the ASE intensity from dyes in LCs depends upon the orientation of the director with respect to the light stripe and polarization, the stripe length-dependent ASE intensity was measured in a configuration, where the ASE intensity is maximum. For all dyes except PM 597, the director is set perpendicular to the light stripe and the polarization of excitation light is set parallel to the director. In this case the radiating dipole of dye is most strongly coupled to the incoming light and the direction of fluorescent emission is directed along the light stripe, i.e. along the direction of maximum stimulated emission. The single pulse pump energy was set well above the ASE threshold, which made the measurement of the optical gain value reliable and accurate [18,19]. All measured ASE data follow an exponential increase of the intensity with increasing stripe length, which is a clear indication of

ASE mechanism [19] and the example of Pyrromethene 580 dye dissolved in 5CB is presented in Figure 4a. The data are presented in log-lin graph, where the data should follow the linear line for long stripe lengths according to small gain model. At very long lengths ($L > 1\text{ mm}$) the ASE peak intensity becomes saturated and the upper limit of the fitting region was chosen at around $\sim 0.6\text{ mm}$, until the intensity still increasing exponentially. On the other side, at very short stripe lengths, there is an error due to: (i) inaccurate determination of the zero of L , i.e. stripe length, (ii) inaccuracy in positioning the stripe with respect to the edge of the glass cell, and (iii) scattering of light of the stripe on imperfections at the cut edge of the glass. The measured ASE intensity at short lengths does not follow the Eq.1, because the origin of this light is not entirely due to ASE.

We have carefully analyzed the influence of the fitting procedure on the value of the optical gain parameter g , as obtained by fitting the measured data to the Eq.1. Several works have pointed to the rather large error and scattering of the g -values (tens of %), especially with respect to the range of the fitting interval[26,29]. While the lower end of the fitting interval of stripe lengths L has little influence on the obtained g -value, the upper end of the fitting interval can significantly alter the obtained g -value. We have therefore determined the upper end of the fitting interval as a point, where the measured data start deviating from the exponential growth in the lin-log plot. We have also slightly shifted the zero of the x-axis in the experimental data, to compensate for the optical irregularities at the cell's edges. This has minor effect on the quality of the fit, as the signal is very weak at short stripe lengths and is of minor statistical relevance. This has been done for all the fitted ASE experimental data sets.

The optical gain parameters were extracted from ASE experiments for different organic dyes dissolved in 5CB, and are presented in Figure 4b. It should be noted that the concentration of all studied dyes in 5CB were equal.

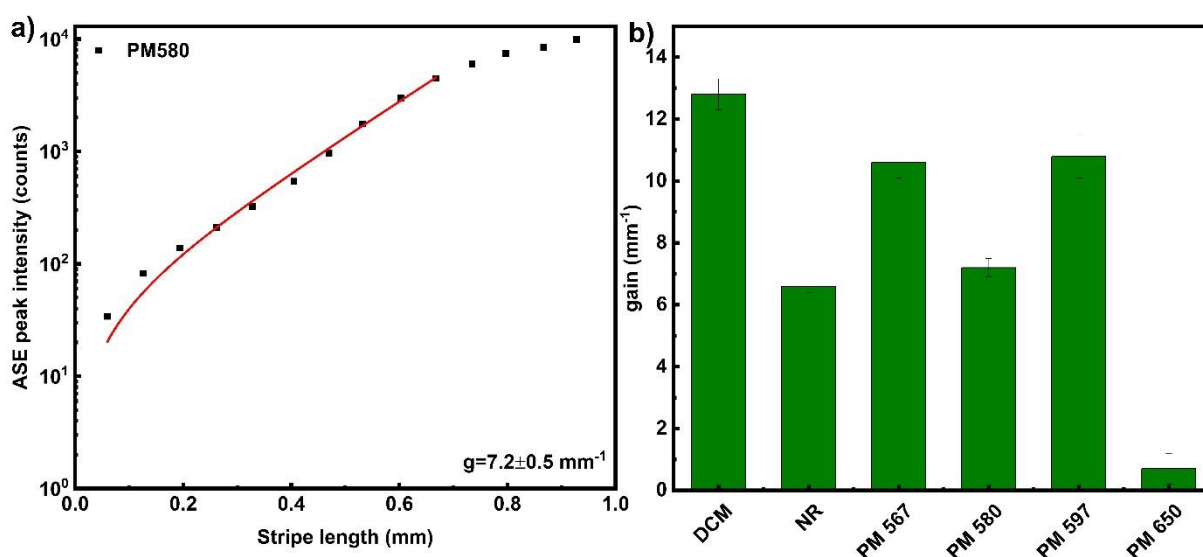


Figure 4. Optical gain parameter extraction from stripe length-dependent ASE peak intensity for (a) 5CB+Pyromethene 580 dye in 19-micrometer thick cell at 1kHz repetition rate and geometry as described in Fig. 3d. The solid line corresponds to the small signal gain model. The data points are ASE peak intensity integrated for 1000 pulses taken at a wavelength of 567 nm. The extracted optical gain parameter is $7.2 \pm 0.5 \text{ mm}^{-1}$. (b) Optical gain parameter extracted by small signal gain model for different dyes (5CB+ dye) in 19-micron thick cell. ASE intensities were integrated over 1000 pulses of 532 nm, 300 fs pulses with energy 0.25 μJ per pulse and the repetition rate of 1 kHz. The concentration of all dyes in 5CB were 0.25 wt%. The peak power density of light stripe was 0.604 GW/cm^2 .

4.1.2. Optical gain of organic polariton material - Anthracene

Room temperature polariton lasing in an organic single crystal microcavity at lower threshold than conventional photon lasing was reported by Cohen et al [30,31]. In this study we used anthracene, a semiconductor organic polariton material as optical gain material. Anthracene is a solid polycyclic aromatic hydrocarbon consisting of three benzene rings, and is the simplest tricyclic aromatic hydrocarbon. Anthracene layer on glass substrate was prepared by drop casting of 2 wt% anthracene dispersion in toluene. To prevent the deposition of undissolved crystals the dispersion is centrifuged before drop casting. The evaporation of toluene resulted in polycrystalline thin film of anthracene, with nearly homogenous layer thickness. To investigate the optical gain, 400 nm wavelength 300 fs pulses with energy of 81 nJ per pulse at a repetition rate of 10 kHz were used to excite the material. The pump beam was linearly polarized perpendicular to the illuminating stripe. Figure 5a shows the evolution of two prominent anthracene emission peaks with increasing stripe length and each spectrum corresponds to emission intensity integrated over 10,000 excitation pulses. The intense emission peak appears at 423 nm and a secondary peak with lower emission intensity appears at 445 nm due to the Davydov splitting that arises from having two inequivalent molecules in a single unit cell [32]. Depending upon the type of the molecular aggregates being J-type or H-type, the emission peak intensity is dominated by primary or the secondary peak [33]. As evident from higher intensity primary peak (Fig. 5a), the J-type aggregates are prominent in anthracene molecular crystals than H-type. We used the most intense ASE peak at 423 nm to extract the optical gain parameter. Figure 5b presents the ASE peak intensity at 423 nm at single pulse pump fluence of 0.576 $\mu\text{J}/\text{cm}^2$ (peak power density of 0.192 GW/cm^2), for different stripe lengths. The extracted gain coefficient is $5.3 \pm 0.5 \text{ mm}^{-1}$. In comparison with gain coefficient from single crystal anthracene film reported in the literature ($\sim 2 \text{ mm}^{-1}$ at pump fluence of 43 $\mu\text{J}/\text{cm}^2$) [30], the polycrystalline anthracene film shows even better gain with lower pump density.

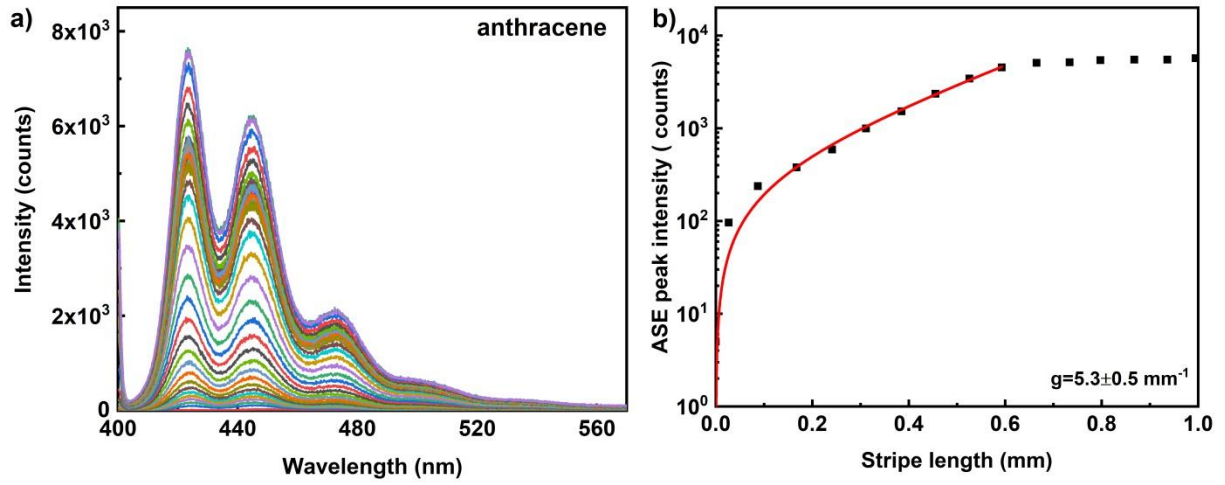


Figure 5. (a) ASE emission spectra from anthracene film at 10kHz repetition rate. The excitation wavelength is 400 nm, 300 fs pulse with energy of 81 nJ per pulse and peak power density of 0.192 GW/cm². The ASE light is integrated over 10.000 pulses at a repetition rate of 10 kHz. Different colour spectrum corresponds to different stripe lengths from 0 – 2mm. (b) The ASE peak intensity as a function of stripe length for anthracene film at 10 kHz repetition rate. The solid line corresponds to the small signal gain model fit in the log-lin scale and thus presents an exponential increase with increasing length. Each data point represents an ASE peak intensity measured for 10.000 pulses taken at a wavelength of 423 nm. The extracted optical gain parameter is $5.3 \pm 0.5 \text{ mm}^{-1}$.

4.1.3. Optical gain of inorganic polariton material: perovskite nanoparticles

The perovskite semiconducting nanoparticles are emerging class of optical gain materials as photonic sources [13,34–36]. Among the perovskite materials, lead-halide perovskites are attracted significant research interest owing to their interesting photophysical properties such as high quantum yield, narrow emission bandwidth and photostability. To compare the optical gain coefficient of organic and inorganic polariton optical gain materials, three lead-halide perovskites CsPbBr_3 , CsPbI_3 and $\text{CsPb}(\text{Br/I})_3$ are investigated. The typical particles are functionalized with organic layer and dispersed in toluene to have 3 wt% of particle concentration. Here the particle sizes are 18, 38 and 40 nm for CsPbBr_3 , CsPbI_3 and $\text{CsPb}(\text{Br/I})_3$ respectively. The perovskite layer on the glass substrate is prepared by drop casting the dispersion in dark at room temperature. The homogenous perovskite layer was excited with 450 nm wavelength 300 fs pulses with energy of 0.167 μJ per pulse at a repetition rate of 1 kHz. The pump beam is linearly polarized in the plane perpendicular to the illuminating stripe. The emission band is narrower with peak wavelengths of 532, 684 and 631 nm for CsPbBr_3 , CsPbI_3 and $\text{CsPb}(\text{Br/I})_3$ respectively. Among three perovskites investigated in this study, CsPbBr_3 has highest quantum yield of 0.9, thus the ASE intensity is highest. Figure 6a shows ASE spectra for CsPbBr_3 at 1 kHz repetition rate with peak power density of 0.53 GW/cm^2 . The ASE peak intensity follows linear dependence for small stripe changes and saturates. The extracted optical gain parameter using small signal gain model (in the linear region) is $18 \pm 2 \text{ mm}^{-1}$.

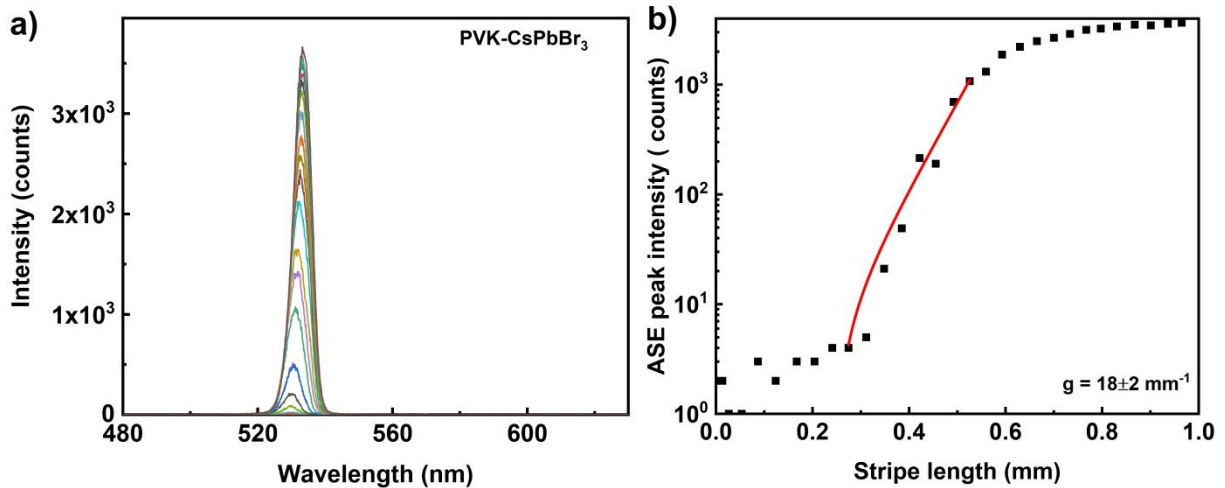


Figure 6. (a) ASE emission spectra from CsPbBr_3 perovskite nanoparticle film. The excitation wavelength is 450 nm, 300 fs pulse with energy of 0.16 μJ per pulse and the ASE light is collected from 1000 pulses at a repetition rate of 1 kHz. Different colour spectrum corresponds to different stripe lengths. (b) Optical gain parameter extraction from the exponential ASE peak intensity as a function of stripe length. The solid line corresponds to the

small signal gain model fit in the log-lin scale and thus presents an exponential increase with increasing length. The scattered data points are ASE peak intensity measured at wavelength of 532 nm. Extracted optical gain parameter is $18 \pm 2 \text{ mm}^{-1}$.

4.1.4. Optical gain of quantum dots and quantum rods

Here, we compare optical gain coefficient of quantum dots (QDs) and rods (QRs). To investigate the optical gain, 30 μl of fluorescent nanomaterial dispersion is drop casted on glass substrate in all cases. The solvent evaporated at room temperature, resulting in thin film of nanoparticles. Typical area of the dried film is $\sim 20 \text{ mm}^2$, whereas the illuminating stripe area is $\sim 0.14 \text{ mm}^2$, and can be considered as homogenous. Figure 7a shows the ASE spectra as function of stripe length from CdSe/ZnS core-shell quantum dot film, prepared by drop casting CdSe/ZnS dispersion with particle size 6.8 nm and 0.5 wt% ($\sim 3 \times 10^{15}$ particles per ml). The thickness of dried films was measured using an Atomic Force Microscope (AFM) and it was in the range 5-8 μm . For excitation wavelength of 532 nm, 300 fs pulse with energy of 0.17 μJ per pulse at a repetition rate of 50 kHz, the ASE intensity appears at $\sim 570 \text{ nm}$. In comparison with the high particle concentration of the dispersion used to prepare QD/QR films, the measured lower ASE intensity is due to the fraction of quantum dots excited, which is $\sim 650 \times 10^9$ particles (at maximum stripe length, assuming homogenous distribution of particles in dried film, typical particle concentration in whole illumination area). As evident from Figure 7b, the peak intensity saturates at a stripe length of 0.5 mm and the exponential dependence of intensity is for short stripe lengths. The extracted optical gain parameter is $30 \pm 3 \text{ mm}^{-1}$. Quantum rods, at similar particle concentrations and pumping conditions, the ASE peak appears at 577 nm and the exponential dependence of emission intensity observed for similar stripe lengths compared to quantum dots. The gain coefficient for CdSe/CdS quantum rod is $23 \pm 4 \text{ mm}^{-1}$ (Figure 8), though the quantum yield is relatively higher for quantum rods (>0.7) than quantum dots (>0.5), similar gain coefficient may attribute to the structural anisotropy of quantum rods. The anisotropic non-spherical luminescent nanocrystals are known to emit linearly polarized light and the emission depends on the orientational ordering of rods, with respect to the pump beam polarizations [37]. We should note that the measured value of g depends upon the optical quality of the deposited film. For this reason, high quality areas of the film should be selected prior to the ASE measurements.

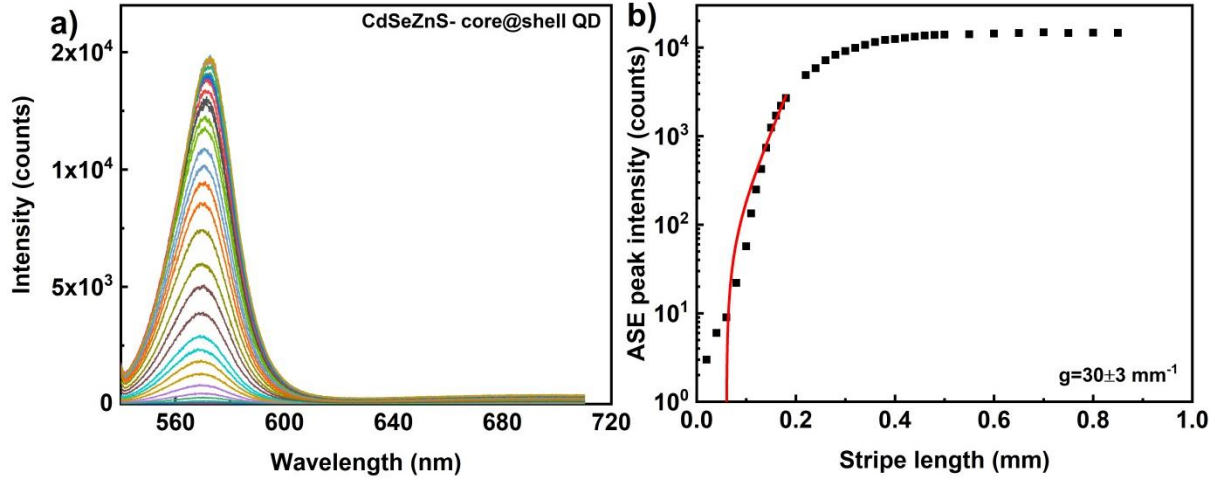


Figure 7. (a) ASE emission spectra from CdSe/ZnS core shell quantum dot film. The excitation wavelength is 532 nm, 300 fs pulses with energy of 0.17 μ J per pulse and the ASE light is collected from 50.000 pulses at a repetition rate of 50 kHz. Different colour spectrum corresponds to different stripe lengths. (b) Optical gain parameter extraction from the exponential ASE peak intensity as a function of stripe length. The solid line corresponds to the linear/small signal gain model fit in the log-lin scale. The scattered data points are ASE peak intensity measured at wavelength of 570 nm. The extracted optical gain parameter is $30 \pm 3 \text{ mm}^{-1}$.

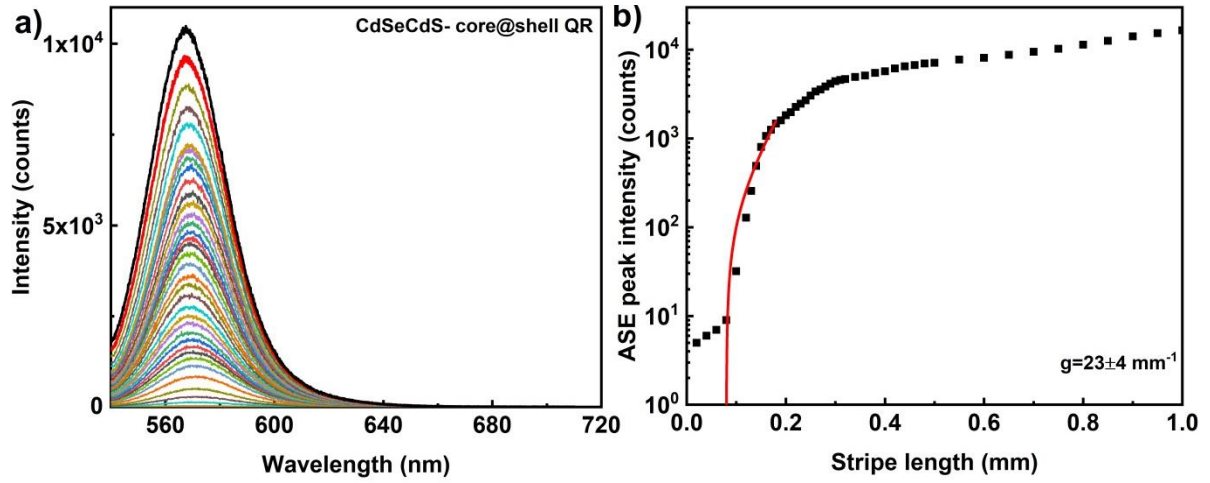


Figure 8. (a) ASE emission spectra from CdSe/CdS core shell quantum rod film. The excitation wavelength is 532 nm, 300 fs pulses with energy of 0.17 μ J per pulse and the ASE light is collected from 50.000 pulses at a repetition rate of 50 kHz. Different colour spectrum corresponds to different stripe lengths. (b) Optical gain parameter extraction from the exponential ASE peak intensity as a function of stripe length. The solid line corresponds to the small signal gain model fit in the log-lin scale. The scattered data points are ASE peak intensity measured at wavelength of 577 nm. The extracted optical gain parameter is $23 \pm 4 \text{ mm}^{-1}$.

4.1.5. Optical gain of nanodiamonds

Nanodiamonds attracted considerable research interest in the recent years, owing to their large optical bandgap, which provides many potential electronic, optical and thermal applications [38–40]. Diamond has a unique combination of properties that is not found in any other material [41,42]. Nanodiamonds are provided in a powder form of diamond nanoparticles with nitrogen vacancy centres, of different sizes and in a form of a dry powder or water dispersion. We have studied two different types of nanodiamonds, the NV nanodiamonds and NVN nanodiamonds. They both act as fluorescent emitters-colour centres, but they are different in terms of the structure, the excitation wavelength and the emitted fluorescence peak wavelength. NV nanodiamonds have a single nitrogen (N) vacancy centre (NV)⁻ that absorbs strongly at ~560 nm and efficiently emits fluorescence at ~700 nm (deep red) [42]. NV nanodiamond films on the glass substrate were prepared by drop-casting fluorescent nanodiamonds dispersed in acetone. The thickness of these films measured by the AFM is around 2 μm and the surface is only 50% covered with diamonds. For this reason, we also performed ASE experiments on water dispersion of NVN nanodiamonds. These materials have a vacancy that is formed around two N atoms in close proximity, and they emit the fluorescent light in green part of the spectrum. We used commercially available Carboxylated nanodiamonds containing NVN centers with green fluorescence from synthetic type Ib diamond in DI water, the average particle size of 120 nm (Adámas Nano) in the optical gain measurements. The dispersion appears as a milky liquid, strongly scattering ambient light because of the large refractive index of a diamond. The water-based dispersion is filled in a 7 μm thick cell and excited with 488 nm, 300 fs pulse of energy 30 nJ, and the repetition rate was 100 kHz. The optical quality in terms of homogeneity of optical gain centres is expected to be much better compared to dried NV films.

Figure 9a presents the ASE emission peak as function of stripe length from nitrogen vacancy (> 900 NV/ nanoparticle) type aminated fluorescent nanodiamond film (particle size 100 nm). The film was excited with 532 nm, 300 fs pulses of single pulse energy of 70 nJ and at a repetition rate of 100k Hz. Compared to polariton particles, nanodiamonds are relatively less bright, because of low volume concentration of NV centers. An increased brightness has been reported by taking larger particle size and defect concentration [43,44]. The ASE spectra are shown in Fig 9a, and correspond to an emission from 10⁵ pulses. The optical gain parameter extracted from the ASE curve in Fig. 9b is $g \sim 5 \pm 1 \text{ mm}^{-1}$. The pumping conditions (wavelength and power), particle concentration, emission wavelength and measured optical gain parameter for different solid state materials are summarized in Table 4.

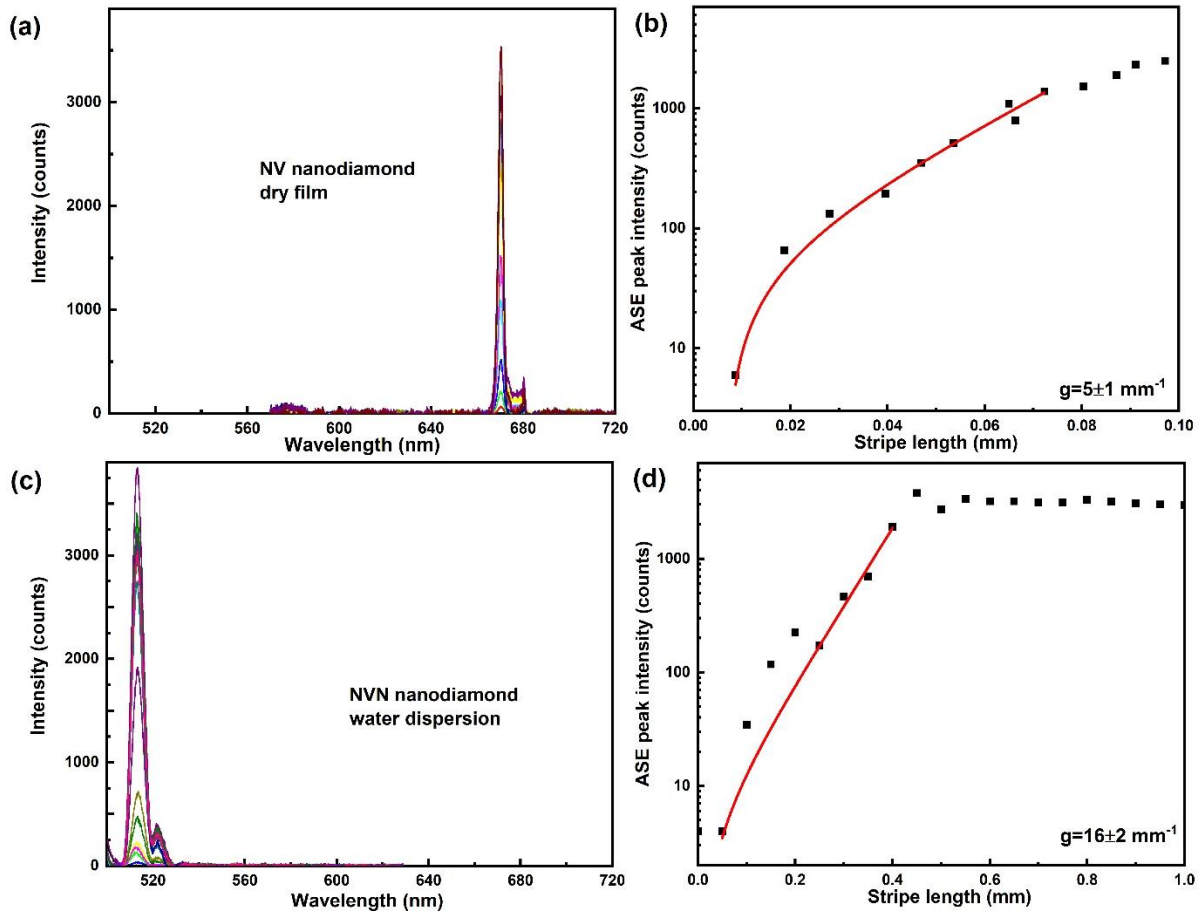


Figure 9. (a) ASE emission spectra from NVN fluorescent nanodiamond film. The excitation wavelength is 532 nm, 300 fs pulses with energy of 70 nJ per pulse and the ASE light is collected from 100.000 pulses at a repetition rate of 100 kHz. Different colour spectrum corresponds to different stripe lengths. (b) Optical gain parameter extraction from the exponential ASE peak intensity as a function of stripe length. The solid line corresponds to the small signal gain model fit in the log-lin scale and thus presents an exponential increase with increasing length. The scattered data points are ASE peak intensity measured at wavelength of 670 nm. Extracted optical gain parameter is $5 \pm 1 \text{ mm}^{-1}$. (c) ASE emission spectra from Green FND (NVN centres) fluorescent nanodiamond dispersion. The excitation wavelength is 488 nm, 300 fs pulses with the energy of 30 nJ per pulse, and the ASE light is collected from 100.000 pulses at a repetition rate of 100 kHz. Different colour spectrum corresponds to different stripe lengths. (d) Optical gain parameter extraction from the exponential ASE peak intensity as a function of stripe length. The solid line corresponds to the small signal gain model fit in the log-lin scale and thus presents an exponential increase with increasing length. The scattered data points are ASE peak intensity measured at a wavelength of 513 nm. Extracted optical gain parameter is $16 \pm 2 \text{ mm}^{-1}$. L_0 is set as 0.01mm

Figure 9c shows the broad fluorescent emission spectra from water dispersion of NVN nanodiamonds, with a peak emission of $\sim 513 \text{ nm}$. Figure 9d, shows ASE peak intensity at 513 nm as a function of stripe length. Each data point corresponds to emissions from 10^5 pulses. Compared to dried NV-type red fluorescence diamond film, the NVN-type green fluorescence nanodiamonds in dispersion, have a higher optical gain of 16 mm^{-1} .

4.1.6 Fluorescent silica nanobeads

We have used commercially available monodispersed fluorescent nanobeads with average particle size of 25 nm (Atto 565, Hiq-Nano). Carboxylic acid group functionalized water-based dispersion of red fluorescent nanobeads is drop casted on glass slide, to make homogenous dry film. The film is excited with 570 nm, 300 fs pulse of energy 88 nJ, peak power density of 0.208 GW/cm² and the repetition rate was 50 kHz. Broad fluorescence emission is observed with peak emission ~590 nm (Figure 10 a). Fig 10b, shows ASE peak intensity at 590 nm as function of stripe length. Scattered data corresponds to emission from 5×10^4 pulses. Compared to quantum dots and rods, silica nanobeads have higher optical gain 8.5 mm⁻¹. However, the broader ASE band and emission intensity is lower (lower quantum yield) compare to other nanoparticle optical gain materials investigated.

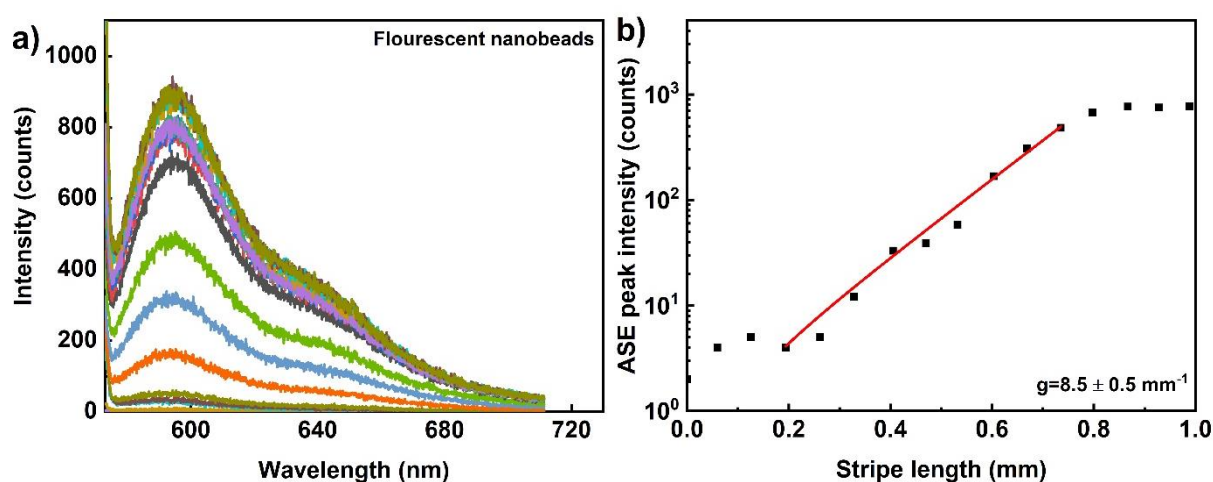


Figure 10. (a) ASE emission spectra from dyed silica nanoparticle film. The excitation wavelength is 570 nm, 300 fs pulses with energy of 88.2 nJ per pulse, peak power density of 0.208 GW/cm² and the ASE light is collected from 50,000 pulses at a repetition rate of 50 kHz. Different colour spectrum corresponds to different stripe lengths. (b) Optical gain parameter extraction from the exponential ASE peak intensity as a function of stripe length. The solid line corresponds to the small signal gain model fit in the log-lin scale and thus presents an exponential increase with increasing length. The scattered data points are ASE peak intensity measured at wavelength of 590 nm. Extracted optical gain parameter is $8.5 \pm 0.5 \text{ mm}^{-1}$.

4.2. Photostability

4.2.1 Photostability of fluorescent dyes, polariton materials and nanomaterials

The photo-stability of an optical gain material was determined by measuring the single pulse peak emitted fluorescence as a function of the number of excitation pulses with predetermined energy per pulse. Depending upon the pumping conditions (pulse energy and duration, stripe length) and the intrinsic properties of optical gain medium, the excess energy delivered during the excitation process results in photo-bleaching. This means that the

intensity of emitted fluorescent light diminishes with the number of excitation pulses. It is well known that each fluorophore/polariton can be photo-bleached after certain number of excitation-emission cycles [45,46]. Different methods were established to characterize the photo-stability, (i) measuring the amount of energy deposited to the medium before its luminescence or lasing intensity reduced to half of the initial value, (ii) quantifying the average number of photons emitted by a molecule till it photobleaches (iii) measuring the photo-degradation rate (photobleaching half-life). Here we quantify the photo-stability by measuring the photo-bleaching half-life in terms of the number of applied excitation pulses of fixed energy. The photo-bleaching half-life number $N_{1/2}$ is therefore the number of excitation pulses needed to reduce the emission peak intensity to one-half of the initial intensity.

We have determined the photo-stability of all the discussed materials by continuously measuring ASE peak intensity from samples at stripe length 1.40 mm over period of time at given pump energy and fixed repetition rate. In all cases studied, except for nanodiamonds, the emitted fluorescence light intensity decays over time. In the continuation, we discuss each material in more detail.

The photo-bleaching experiments in 5CB planar cells with different laser dyes, which are shown in Figure 11, show a single exponential decrease of intensity over the number of pulses applied, as described by Eq. (2). Among the laser dyes, pyromethene dyes exhibit the highest photo-stability. On the other hand, the photo-bleaching experiments on polariton fluorescent materials, shown in Figure 12, show double exponential time-decay, as described by Eq. (3):

$$I = I_{\infty} + I_0 e^{-N/N_e} \quad (2)$$

$$I = I_{\infty} + I_1 e^{-N/N_{1e}} + I_2 e^{-N/N_{2e}} \quad (3)$$

Here, I_0 and I_{∞} are the initial intensity and intensity after infinity numbers of excitation pulses ($I_{\infty} \geq 0$). I_1 and I_2 are the initial intensities at which intensity each decay process starts for the two-step decay process. N_e , N_{1e} and N_{2e} are the decay constants, i.e. number of excitation pulses needed to reduce the initial intensity to $I = I_0/e$ and the half-life number is calculated by $N_{1/2} = \ln(2) \times N_e$.

Figure 11 shows the photostability of laser dyes obtained for excitation wavelength 532 nm, power density of 0.604 GW/cm² and the ASE peak intensity collected at a repetition rate of 1 kHz and 10 sec exposure time (each data point is collected after 10⁴ pulses). Intensity decay of most of the dyes follow single exponential decay, except PM 580 and 597, which follows double exponential decay. As evident from the figure 11, pyromethene dyes show slower decay compared to DCM and Nile red dyes. Among the four pyromethene dyes

investigated PM 565 has the highest half-life pulses $\sim 10^7$ pulses, while the half-life pulses for PM 580 and PM 597 is as low as $\sim 6 \times 10^6$ pulses. The emission intensity for PM 650 is lower than all other dyes, and the feeble intensity decays rapidly. To summarize, the pyrromethene dyes are having better photostability than other investigated dyes.

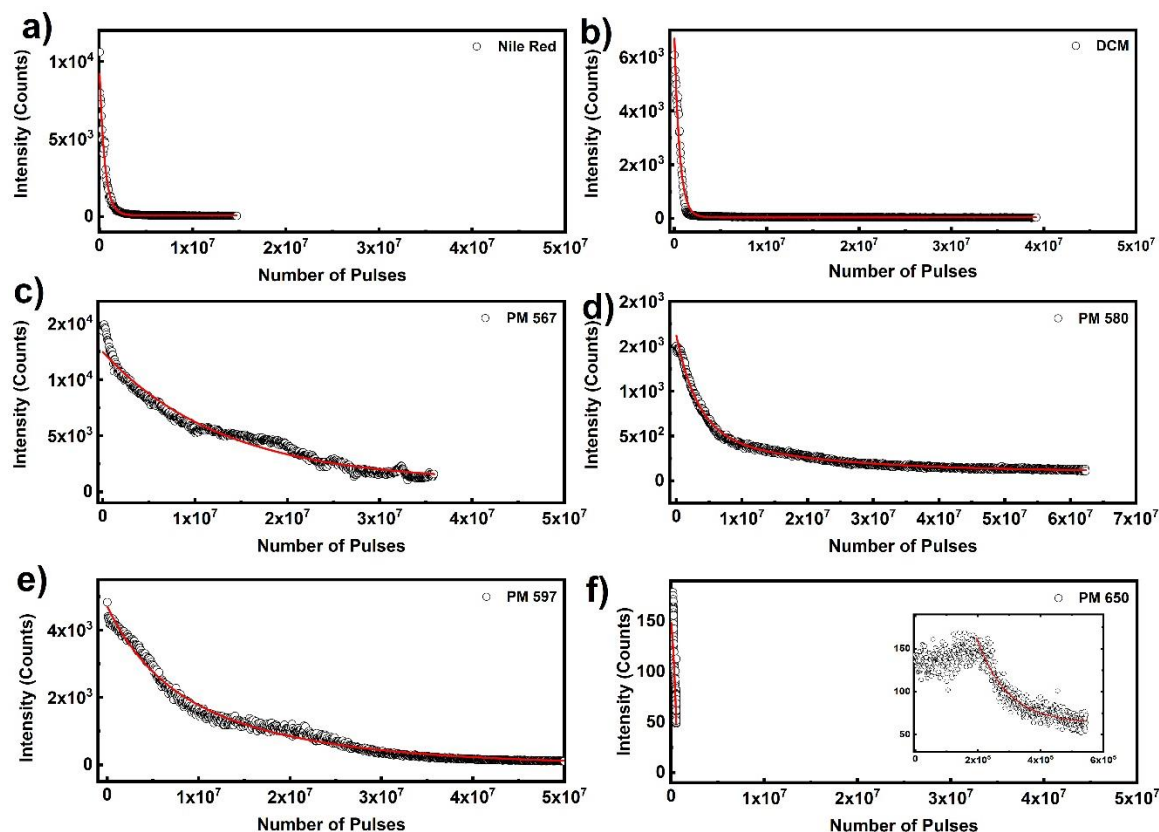


Figure 11. ASE peak intensity decay for 5CB + dye in 19 μm planar cell. The excitation wavelength is 532 nm, 300 fs pulse peak power density of 0.604 GW/cm² and the ASE peak intensity is collected for 10^4 pulses at a repetition rate of 1 kHz. (a-c and f) The solid line corresponds to a single exponential fit and (d, e) solid line corresponds to the double exponential decay fit.

While the organic laser dyes typically show single exponential decay mode of photobleaching, the nanoparticle optical gain materials are rather different. As shown in Fig. 12, the intensity over number of excitation pulses show two exponential decay for silica nanobeads, QRs, QDs and perovskite CsPbBr₃, while in the case of perovskites CsPbI₃ and CsPb(Br/I)₃ the ASE intensity is very weak and photostability can be described by one exponential decay. The most stable are QDs and QRs, where the fast decay is characterized by around 10^7 pulses and the slow decay lasts for around 10^9 pulses. Next are silica nanobeads, which have shorter half-life, around 10^6 pulses for faster and 10^8 pulses for slower decay. Among perovskites the most stable are CsPbI₃ particles with half-life 8×10^8 pulses, but they exhibit smaller ASE intensity. The stability of CsPbBr₃ particles was also described with two bleaching processes, which are characterized with relatively fast two decay processes with half-life 10^6 and 10^7

pulses, respectively, while the CsPb (Br/I)₃ particles are the least stable with decay constant of around 10^7 pulses.

The detailed data for all nanoparticles are collected in Table 4.

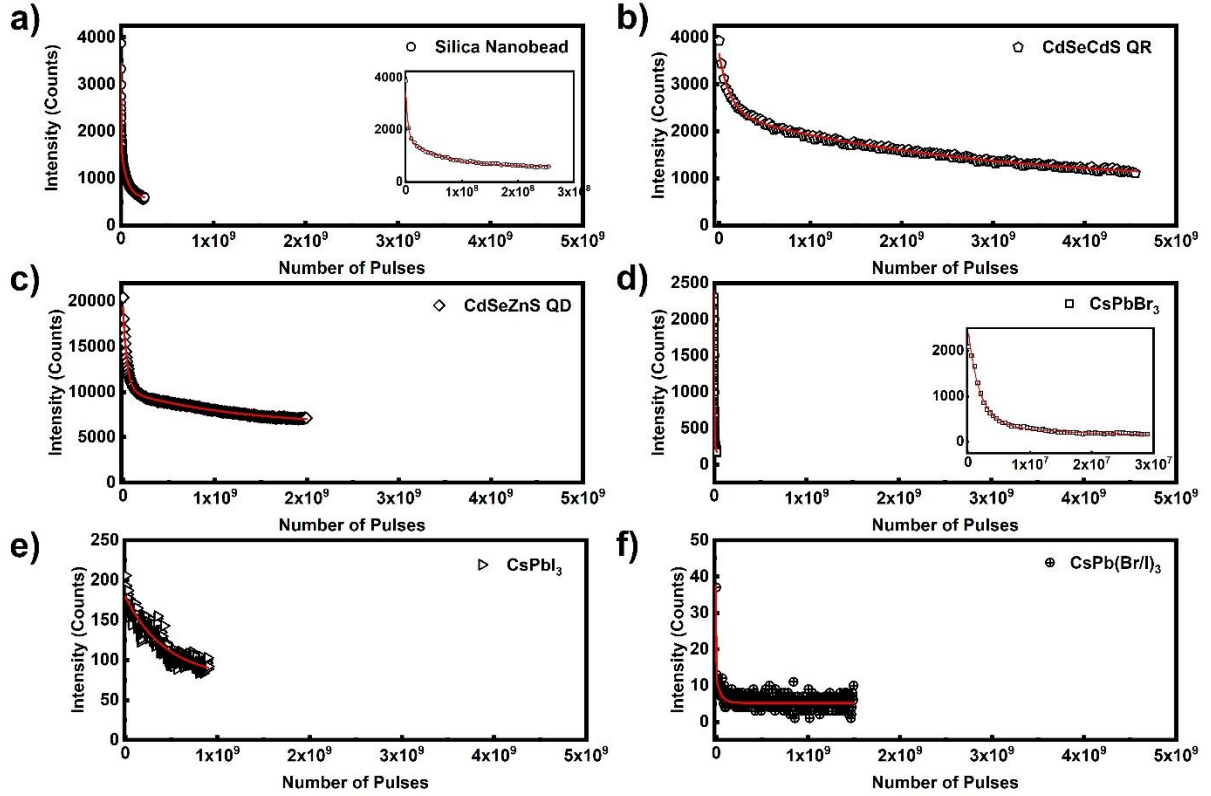


Figure 12. ASE peak intensity decay as a number of applied laser excitation pulses for silica nanobeads, QRs and QDs, and room temperature polariton film. The sample is excited with 300 fs pulse of different wavelength and peak power density as mentioned in Table 4. (a-d) solid lines correspond to double exponential decay fit and (e,f) single exponential decay fit to the intensity.

4.2.2. Photostability of Nanodiamonds with NV and NVN centers

One of the unique properties of fluorescent nanodiamonds are nitrogen vacancy (NV) defect centres, which act as an nitrogen ion and a lattice vacancy embedded in an inert diamond solid matrix, thereby providing an exceptional photostability [42,47–49]. The luminescence of the NV centre is extremely robust, with no bleaching or blinking under normal conditions. Figure 13 shows the time dependence (i.e. the number of applied pulses at fixed repetition rate) ASE intensity under pulsed excitation at the repetition rate of 100kHz and 5 sec of exposure. Out of all the materials studied in this work, only nanodiamonds with NV and NVN centres show ideal photostability over 10^{10} applied excitation pulses. For a 100 kHz repetition rate of the excitation laser, the emitted fluorescence intensity is stable over ~24 hours of illumination ($>10^{10}$ pulses), with no sign of even the slightest bleaching.

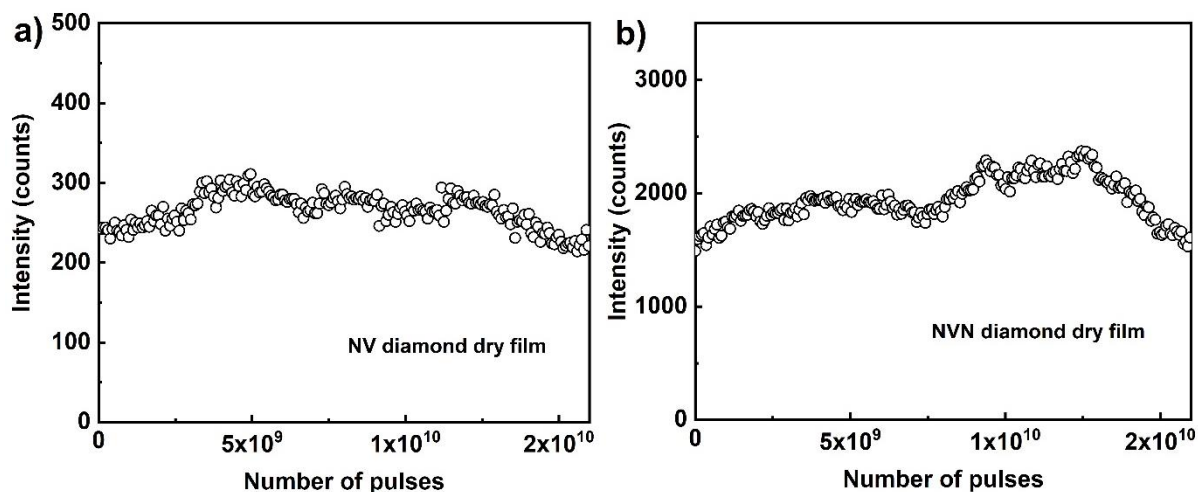


Figure 13. ASE peak intensity decay for NV (a) and NVN (b) fluorescent nanodiamond film. The excitation wavelength is 532 nm, 300 fs pulse with 0.16 GW/cm² peak power density and the ASE peak intensity is collected from 670 nm emission peak, for every 5×10⁵ pulses at a repetition rate of 100 kHz for NV fluorescent nanodiamond film. The excitation wavelength is 488 nm, 300 fs pulse with 99.5 MW/cm² peak power density, and the ASE peak intensity is collected from a 513 nm emission peak, for every 10⁶ pulses at a repetition rate of 100k Hz for NVN fluorescent nanodiamond film.

Table 3. Summary of fluorescence parameters and bleaching properties of organic dyes. Optical gain and photostability values are measured for 0.25 wt% of dye dispersed in planar aligned 5CB matrix. The excitation source is 532 nm, 300 fs pulse with power density 0.604 GW/cm² in all experiments.

Parameter	PM 567	PM 580	PM 597	PM650	DCM	NR
Fluorescence life time	213 ns	218 ns	203 ns	220 ns	2 ns	2.8 ns
Quantum efficiency	0.99 (in methanol)	0.90 (in methanol)	0.77(in methanol)	0.54 (in methanol)	0.43 (in methanol)	0.7 (in dioxane)
Dichroic order parameter	0.25	0.30	0.29	0.36	0.32	0.28
Optical Gain	10.6 ± 0.5 mm ⁻¹	7.2 ± 0.3 mm ⁻¹	10.8 ± 0.7 mm ⁻¹	0.7 ± 0.5 mm ⁻¹	12.8±0.5 mm ⁻¹	6.6 ± 0.2 mm ⁻¹
Pump Power density	0.604 GW/cm ²	0.604 GW/cm ²	0.604 GW/cm ²	0.604 GW/cm ²	0.604 GW/cm ²	0.604 GW/cm ²
λ ASE Peak	557 nm	565 nm	576 nm	650 nm	602nm	621 nm

Photo-stability $N_{1/2}$ (Half-life pulses)	$\sim 1 \times 10^7$	2×10^6 (70%) and 1.3×10^7 (30%)	3.3×10^6 (37%) and 1.3×10^7 (63%)	$\sim 5 \times 10^4$	$\sim 3.9 \times 10^5$	3.9×10^5
--------------------------------------------------------	----------------------	------------------------------------------------------------	-----------------------------------------------------------------	----------------------	------------------------	-------------------

Table 4. Summary of fluorescence parameters and photo bleaching properties of QDs, QRs, room temperature polaritons and NV diamonds. Optical gain and photostability values are measured in dried films. If the photostability is described by two decay processes, both half-life numbers and their relative contributions are presented.

Parameter	CdSe/ ZnS QD	CdSe/ CdS QR	CsPbBr ₃	CsPbI ₃	CsPb (Br/I) ₃	silica beads	Anthracen e	NV Fluorescent diamond	NVN Green Fluorescent diamond
Size	6.8 nm	5x30 nm	18 nm	38 nm	40 nm	25 nm	n.a.	100 nm	120 nm
Quantum eff.	> 50 %	> 70%	90%	78%	80%	n.a.	n.a.	n.a.	n.a.
Concentration	0.5 wt%	0.5 wt %	3 wt%	3 wt%	3 wt%	1 wt%	2 wt%	0.1 wt%	0.1 wt%
Optical Gain	$9 \pm 3 \text{ mm}^{-1}$	$11 \pm 3 \text{ mm}^{-1}$	$25 \pm 5 \text{ mm}^{-1}$	$6.0 \pm 0.3 \text{ mm}^{-1}$	$2.0 \pm 0.3 \text{ mm}^{-1}$	$8.5 \pm 0.4 \text{ mm}^{-1}$	$5.3 \pm 0.5 \text{ mm}^{-1}$	$5 \pm 1 \text{ mm}^{-1}$	$16 \pm 2 \text{ mm}^{-1}$
$\lambda_{\text{excitation}}$	532 nm	532 nm	450 nm	450 nm	450 nm	570 nm	400 nm	532 nm	488 nm
Peak power density	0.403 GW/cm ²	0.403 GW/cm ²	0.53 GW/cm ²	0.53 GW/cm ²	0.53 GW/cm ²	0.208 GW/cm ²	0.192 GW/cm ²	0.166 GW/cm ²	0.007 GW/cm ²
Repetition rate	50 kHz	50 kHz	1kHz	50 kHz	100kHz	50kHz	10 kHz	100 kHz	100 kHz
$\lambda_{\text{ASE Peak}}$	567 nm	557 nm	532 nm	684 nm	631 nm	590 nm	423 nm	670 nm	513 nm
Photo-stability $N_{1/2}$ (Half-life pulses)	3.5×10^7 (52%) and 3.8×10^9 (48%)	1×10^8 (86%) and 3.8×10^9 (14%)	$\sim 10^6$ (86%) and 2×10^7 (14%)	$\sim 8 \times 10^8$	$\sim 2 \times 10^7$	$\sim 2 \times 10^6$ (60%) and 1.5×10^8 (40%)	$\sim 10^7$ (63%) and $\sim 9 \times 10^7$ (37%)	$> 10^{10}$	$> 10^{10}$

4.2.3 Peak power density-dependent photobleaching of selected materials

The conventional dye lasers require intensive pulsed light excitation (pumping), so we also measured the effect of bleaching on the ASE intensity at different power densities of the pumped beam for some selected optical gain materials, PM580, CdSe/ZnS quantum dots and Anthracene.

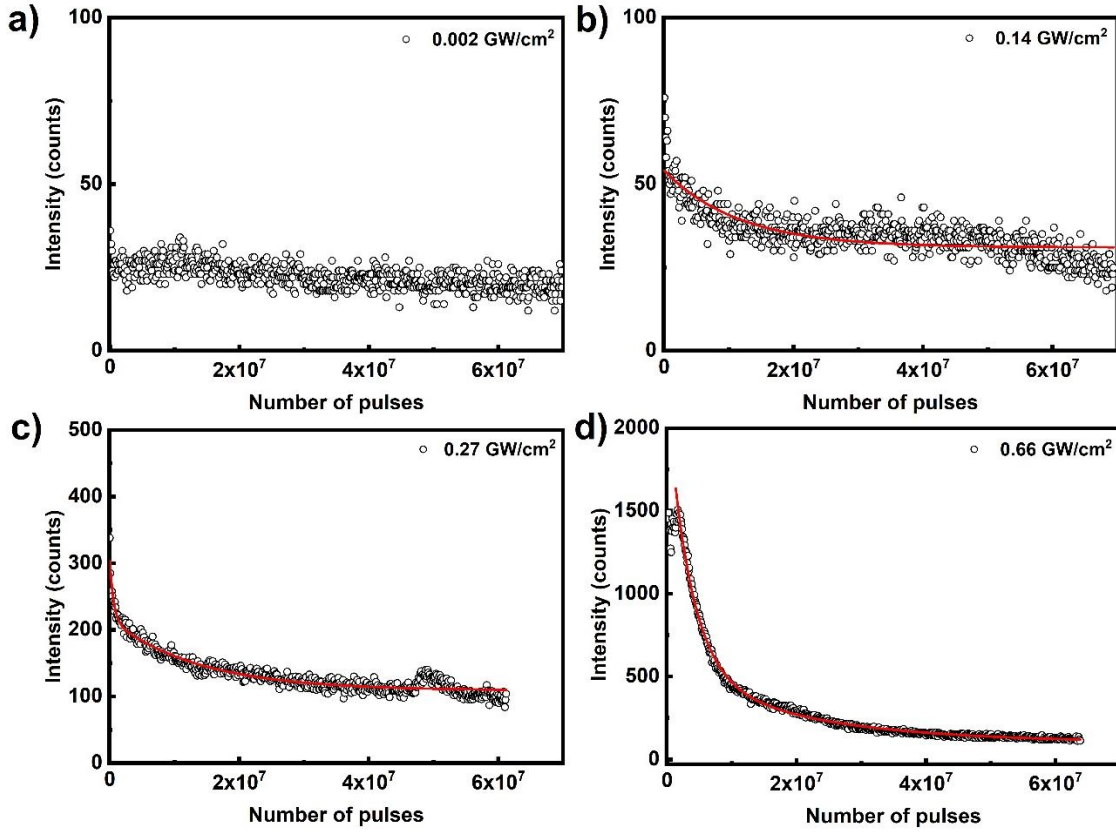


Figure 14. Peak power density dependent ASE peak intensity decay for PM 580 dye in 19 μm thick planar cell of 5CB. The scattered data points are ASE peak intensity is collected from at a repetition rate of 1k Hz, with excitation wavelength is 532 nm, 300 fs pulse. The solid lines correspond to a single exponential decay (b) and double exponential decay model (c & d).

Photobleaching of the dye depends on the pump power and dye concentration. Hence, the dye concentration, duration of pumping and repetition rate were kept the same while the pump power changed as seen in Figure 14, to evaluate the photostability of PM 580 as function of the excitation power. For these experiments, pump beam polarization was kept perpendicular to the exciting stripe, i.e. for maximum excitation and emission. Figure 14 shows that the emission is follows single decay process and the rate of decay increases with pump powers. At the low pump power density, data were fit with single exponential decay model (Equ. 2). However, for higher pump power densities, intensity decay data are well described by the double exponential decay model as described in

Equ. 3. The parameters of the photobleaching curves are listed in Table 5. At the pump power 0.66 GW/cm² (fig. 14 d), 78% of the total decay is via the fast mode with half-life of 2.5×10^6 pulses and the remaining 22% intensity decays via slow decay mode with half-life of 10^7 pulses. Though the intensity decay follows two decay modes, at low pump power (0.27 GW/cm²) both modes are equally contributing the bleaching process while at high pump power the initial fast decay mode describes the decay process.

Table 5. Photobleaching parameters for PM 580

Peak power density (GW/cm ²)	Amplitude (counts)		Half-life (pulses)	
	I ₁	I ₂	N _{1/2}	N _{2/2}
0.14	23	-	$(1.6 \pm 1) \times 10^7$	-
0.27	89	107	3.9×10^5	1×10^7
0.66	1621	448	2.5×10^6	1.3×10^7

Figure 15 shows the decay of the fluorescence intensity from anthracene film at different pump power densities. We found that a double exponential fit using Eq. (3) describes well the observed decay. The sample was photobleached with 400 nm, 300 fs pulses. Except for very low pump power density of 0.002 GW/cm² the intensity decays double-exponentially over time, indicating that there are at least two photobleaching processes. Similar double exponential decay photobleaching was observed in tetracene compounds [50].

The parameters of the anthracene photobleaching curves are listed in Table 6. Regardless of different power densities, the photobleaching follows two decay modes. At the 0.026 GW/cm², 28% of the total decay process is via the first mode (1.4×10^7 pulses) and remaining 72 % follows the second mode (1.2×10^8 pulses). As the power density increases to 0.102 GW/cm², the photobleaching process is predominant (56%) by the initial fast decay with half-life of 1.2×10^7 pulses, followed by slow second mode with half-life off 9×10^7 pulses (44%). At pump power 0.192 GW/cm², similar intensity decay behaviour is observed, the initial intensity decays rapidly with half-life of 1.2×10^7 (63%) followed by a slow second decay with longer half-life of 9.1×10^7 (37%).

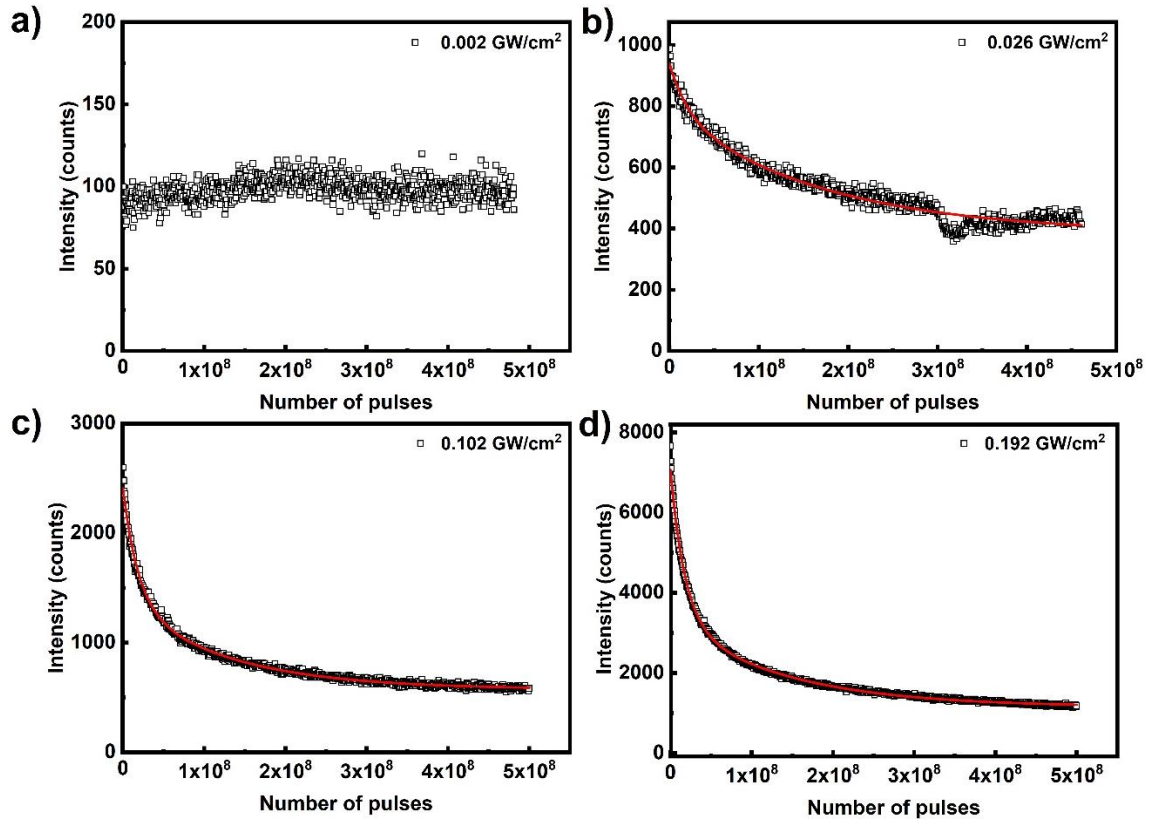


Figure 15. Peak power density dependent ASE peak intensity decay for Anthracene film. Scattered data points are the emission peak intensity as a function of excitation pulses, measured at different pump fluence for Anthracene film. The excitation source is Origami OPA 400nm, 300 fs pulse with different peak power densities at 10 kHz repetition rate. The solid lines correspond to the double exponential decay as described by Eq. 3.

Table 6. Photobleaching parameters for anthracene

Peak power density (GW/cm ²)	Amplitude (counts)		Half-life (pulses)	
	I ₁	I ₂	N _{1/2}	N _{2/2}
0.026	156	400	1.4×10^7	1.2×10^8
0.102	1030	807	1.2×10^7	9×10^7
0.192	3730	2199	1.2×10^7	9.3×10^7

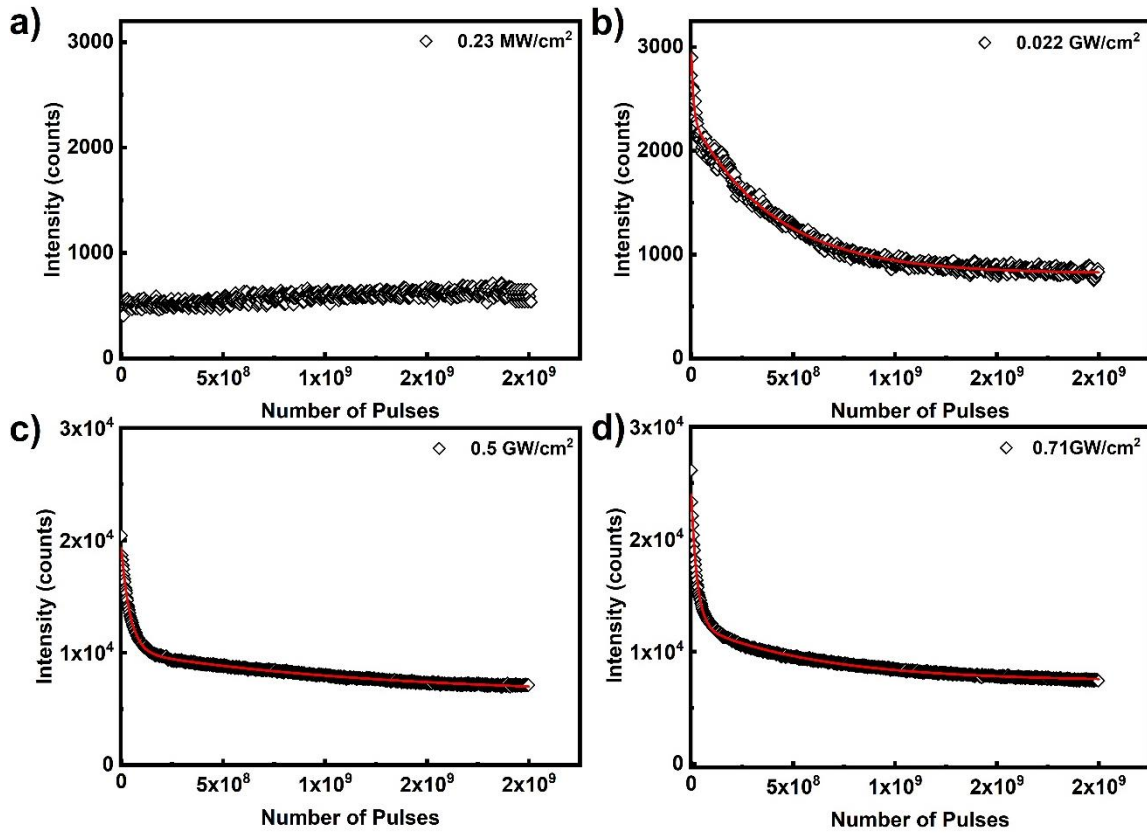


Figure 16. Peak power density dependent ASE peak intensity decay for CdSe/ZnS core shell quantum dot film. The scattered data points are emission peak intensity as a function of excitation pulses, measured at 50kHz repetition rate with excitation source Origami OPA 532nm, 300 fs pulse with different peak power densities. The solid lines correspond double exponential decay mode as described by eq.3.

Figure 16 shows pump intensity decay over time for CdSe/ZnS core shell quantum dot film, excited at 532 nm of 300 fs pulses. The parameters of the emission intensity fitted to double exponential decay are listed in Table 7. Similar to anthracene, quantum dot photobleaching is double exponential decay process. Among the two mode decay processes, predominant decay mode is depending on the pump power density. As evident from Fig.16 (c,d) at high pump powers, the fast decay process dominates the photo-bleaching processes. At lower pump power, the second (slow) mode dominates, while at higher pump power the first (fast) mode dominates the decay process. At the lowest power density, around 30% of the photobleaching process is mediated by the initial fast decay with half-life of 7×10^6 pulses and the remaining 70% is via second slow decay process with half-life 3×10^8 . When the pump power density increases to 0.5 GW/cm^2 , the decay process is predominated by fast decay processes (70%), with half-life of 3.5×10^7 and remaining 30% is mediated by the second slow decay mode with half-life of 9×10^8 pulses. At maximum pump power density of 0.71 GW/cm^2 the half-life of the decay rate is comparable to 0.5 GW/cm^2 . However, the two-decay process half-life are 2×10^7 (70%) and 4×10^8 (30%) pulses.

Table 7. Photobleaching parameters for CdSe/ZnS quantum dots

Peak power density (GW/cm ²)	Amplitude (counts)		Decay constant (pulses)	
	I ₁	I ₂	N _{1/2}	N _{2/2}
0.022	624	1503	0.7×10 ⁷	2.8 ×10 ⁸
0.5	9239	3924	3.5×10 ⁷	9 ×10 ⁸
0.71	11591	5074	2×10 ⁷	4 ×10 ⁸

Pyromethene 580, anthracene and CdSe/ZnS quantum dots follow similar power density dependent photobleaching characteristics, the intensity decays via double decay modes. Anthracene and CdSe/ZnS quantum dots follow double decay process, the power density dependence on decay modes are same. In both cases of Anthracene, and CdSe/ZnS quantum dots at lower pump power, the second (slow) mode dominate while at higher pump power the first (fast) mode dominates the decay process.

5. Conclusions

We have investigated optical gain and photobleaching of several classes of fluorescent materials: (i) organic fluorescent dyes, (ii) inorganic fluorescent materials, and (iii) NV nanodiamonds. In terms of practical application as optical gain materials for liquid crystal microlasers, fluorescent organic dyes have several important advantages. They can easily be dissolved and mixed with any LC, giving bright fluorescence and superior optical gain. However, in terms of long-term use in any practical device, where dyes would be exposed to high optical fluence, fluorescent organic dyes are not useful due to their weak photostability. This serious drawback is even more pronounced when a LC with dissolved dye is confined to a small, ~20 μm droplet, embedded in another immiscible fluid or a polymer. Our experiments show that the life time of the most stable dye pyromethene 580 is shortened by nearly two orders of magnitude, when the material is confined into a LC droplet. This imposes serious restrictions even to laboratory studies of lasing from dye-doped LC droplets, and the repetition rate of the excitation laser has to be kept low (i.e. 1-10 Hz) to have any control over the experiment. For dye-doped LC microlasers, pyromethene dyes offer wider emission wavelengths and are better in terms of stability compared to DCM and Nile Red dyes. Among the laser dyes DCM yields slightly higher optical gain coefficient than pyromethene dyes, but pyromethene dyes outperform DCM in terms of longer photostability.

In addition to dyes, optical gain parameters and lifetime were determined for an organic and few inorganic polariton materials. Though the anthracene is organic molecule like other laser dyes, it forms molecular crystals

and behaves as room temperature polariton. Among the tested inorganic optical gain materials, perovskite CsPbBr_3 yield the highest optical gain coefficient, but this material has rather low photostability in comparison to QDs and QRs, which are superior to any other inorganic fluorescent material, except for NV and NVN nanodiamonds.

Among all optical gain materials studied, nanodiamonds stand unique, exhibiting no change in emission intensity over time. For example, under same excitation wavelength, at relatively low excitation power (0.022 GW/cm^2) ASE intensity drops to half of the initial value in $\sim 10^8$ pulses for CdSe/ZnS quantum dots, while nanodiamonds at pump power 0.16 GW/cm^2 are photostable over $>10^{10}$ pulses, showing no signs of degradation up to this number of illuminating pulses.

Finally, we should comment on the long-time fluorescence, when the gain material is exposed to a large number of very intense optical pulses. For example, it might be misleading to conclude from Figure 16.d that CdSe/ZnS core shell quantum dots show a significant fluorescence even at very large number of applied optical pulses. The fitting parameters for the curve in panel (d) show that the baseline number of counts is ~ 7.300 (i.e. the photon counts for infinitely long illumination). This baseline fluorescence in panel (d) can be compared to the fluorescence in panel (a) by taking into account very different excitation power density. Whereas in panel (a) the excitation power density was 0.23 MW/cm^2 , the excitation power density for data in panel (d) was 0.71 GW/cm^2 . This is for a factor of 3.100 higher intensity, which should give $\sim 1.500.000$ emitted photons, if the sample was not bleached. In reality, we get only 7.300 photons emitted per excitation pulse. This gives us a rough estimate that only 0.4% of photon emitters have survived the very strong light irradiation. It is quite clear that CdSe/ZnS core shell quantum dots are in fact not photostable and cannot be used in laser applications, which require robustness and stable emission in very strong light.

We can safely conclude from this study that NV and NVN nanodiamonds are superior optical gain material in terms of extremely long lifetime, and they exhibit moderate optical gain coefficient. There are two potential drawbacks of NV and NVN nanodiamonds: (i) rather low fluorescent emission from these materials, which is most likely due to rather low number of fluorescent NV centers implanted into these materials. Currently, volume density of NV centers in available NV nanodiamonds is around 900 centers per particle; (ii) difficulties in obtaining well dispersed NV diamond nanoparticles in a LC, as mentioned in the introduction. However, owing to the well-defined emission and excellent photostability, nanodiamonds will most likely be a potential optical gain material for applications in soft matter microphotonic devices. This was also demonstrated in recent publications reporting optical amplification and lasing from NV nanodiamonds and diamonds [51,52].

Declaration of Competing Interest: The authors declare that they have no known competing financial interests or personal relationships that could have appeared to influence the work reported in this paper.

Acknowledgment: This result is part of a project that has received funding from the European Research Council (ERC) under the European Union's Horizon 2020 Research and Innovation Program (Grant agreement No. 884928-LOGOS).

References

- [1] Mowatt C, Morris SM, Song MH, et al. Comparison of the performance of photonic band-edge liquid crystal lasers using different dyes as the gain medium. *J Appl Phys.* 2010;107:1–9.
- [2] Urbas AM, Jacob Z, Dal L, et al. Biomaterials in light amplification. *J Opt.* 2017;033003:31.
- [3] Zhou C, M. Pina J, Zhu T, et al. Quantum Dot Self-Assembly Enables Low-Threshold Lasing. *Adv Sci.* 2021;8:1–7.
- [4] Inoué S, Shimomura O, Goda M, et al. Fluorescence polarization of green fluorescence protein. *Proc Natl Acad Sci.* 2002;99:4272– 4277.
- [5] Gather MC, Yun SH. Bio-optimized energy transfer in densely packed fluorescent protein enables near-maximal luminescence and solid-state lasers. *Nat Commun.* 2014;5:1–8.
- [6] Porotnikov D, Diroll BT, Harankahage D, et al. Low-threshold laser medium utilizing semiconductor nanoshell quantum dots. *Nanoscale.* 2020;12:17426–17436.
- [7] Alvarado-Leaños AL, Cortecchia D, Folpini G, et al. Optical Gain of Lead Halide Perovskites Measured via the Variable Stripe Length Method: What We Can Learn and How to Avoid Pitfalls. *Adv Opt Mater.* 2021;2001773.
- [8] Kumar R, Raina KK. Optical and electrical control of circularly polarised fluorescence in CdSe quantum dots dispersed polymer stabilised cholesteric liquid crystal shutter. *Liq Cryst.* 2016;43:994–1001.
- [9] Morris SM, Ford AD, Pivnenko MN, et al. The effects of reorientation on the emission properties of a photonic band edge liquid crystal laser. *J Opt A Pure Appl Opt.* 2005;7:215–223.
- [10] Lei L, Dong Q, Gundogdu K, et al. Metal Halide Perovskites for Laser Applications. *Adv Funct Mater.* 2021;31:1–21.
- [11] Ichimura M, Ishikawa K. Development of highly fluorescent distyryl dyes for liquid crystal lasers. *Jpn J Appl Phys.* 2019;58:0–6.
- [12] Dietrich CP, Steude A, Tropf L, et al. An exciton-polariton laser based on biologically produced fluorescent protein. *Sci Adv.* 2016;2:1–8.

- [13] Sutherland BR, Sargent EH. Perovskite photonic sources. *Nat Photonics*. 2016;10:295–302.
- [14] Humar M, Ravnik M, Pajk S, et al. Electrically tunable liquid crystal optical microresonators. *Nat Photonics*. 2009;3:595–600.
- [15] Humar M, Mušević I. Surfactant sensing based on whispering-gallery-mode lasing in liquid-crystal microdroplets. *Opt Express*. 2011;19:19836.
- [16] Humar M, Mušević I. 3D microlasers from self-assembled cholesteric liquid-crystal microdroplets. *Opt Express*. 2010;18:26995.
- [17] Ryzhkova A V., Pratibha R, Nikkhou M, et al. Tuneable ferroelectric liquid crystal microlaser. *Liq Cryst*. 2020;47:994–1003.
- [18] Cerdan L, Costela A, Garcia-Moreno I. Variable Stripe Length method for optical gain measurements: Characteristic lengths. 2011 Conf Lasers Electro-Optics Eur 12th Eur Quantum Electron Conf CLEO Eur 2011. 2011;27:1874–1877.
- [19] Shaklee KL, Leheny RF. Direct determination of optical gain in semiconductor crystals. *Appl Phys Lett*. 1971;18:475–477.
- [20] Škarabot M, Mušević I. Direct observation of interaction of nanoparticles in a nematic liquid crystal. *Soft Matter*. 2010;6:5476–5481.
- [21] Ryzhkova A V., Mušević I. Particle size effects on nanocolloidal interactions in nematic liquid crystals. *Phys Rev E - Stat Nonlinear, Soft Matter Phys*. 2013;87:1–12.
- [22] Ryzhkova A V., Škarabot M, Mušević I. Surface charge and interactions of 20-nm nanocolloids in a nematic liquid crystal. *Phys Rev E - Stat Nonlinear, Soft Matter Phys*. 2015;91:1–8.
- [23] Topnani NB, Nagaraja P, Musevic I, et al. Fluorescence intermittency and spatial localization of core-shell quantum rod clusters in an inverse nematic gel. *Phys Rev Mater*. 2020;4:1–10.
- [24] Pandya R, Chen RYS, Gu Q, et al. Microcavity-like exciton-polaritons can be the primary photoexcitation in bare organic semiconductors. *Nat Commun*. 2021;12:1–11.
- [25] Rajendran SK, Wei M, Ohadi H, et al. Low Threshold Polariton Lasing from a Solution-Processed Organic Semiconductor in a Planar Microcavity. *Adv Opt Mater*. 2019;7:1801791.
- [26] Cerdán L. Variable Stripe Length method: influence of stripe length choice on measured optical gain. *Opt Lett*. 2017;42:5258.
- [27] Costela A, García O, Cerdán L, et al. Amplified spontaneous emission and optical gain measurements from pyromethene 567- doped polymer waveguides and quasi-waveguides. *Opt Express*. 2008;16:7587.
- [28] Vellaichamy M, Mušević I. Optical gain and photostability of different laser dyes, quantum dots and quantum rods for liquid crystal micro lasers. *Proc SPIE 12023, Emerg Liq Cryst Technol XVII*, 120230A (3 March 2022); San Francisco, California, United States: SPIE; 2022. p. 17.
- [29] Lange C, Schwalm M, Metzger B, et al. Carrier-depletion in the stripe-length method: Consequences for gain measurement. *J Appl Phys*. 2010;108.

- [30] Kéna-Cohen S, Forrest SR. Room-temperature polariton lasing in an organic single-crystal microcavity. *Nat Photonics*. 2010;4:371–375.
- [31] Sanvitto D, Kéna-Cohen S. The road towards polaritonic devices. *Nat Mater*. 2016;15:1061–1073.
- [32] Davydov SA. *Theory of molecular excitons*. New York: Plenum; 1971.
- [33] Bardeen CJ. The structure and dynamics of molecular excitons. *Annu Rev Phys Chem*. 2014;65:127–148.
- [34] Su R, Fieramosca A, Zhang Q, et al. Perovskite semiconductors for room-temperature exciton-polaritonics. *Nat Mater*. 2021;20:1315–1324.
- [35] Zhang Q, Shang Q, Su R, et al. Halide Perovskite Semiconductor Lasers: Materials, Cavity Design, and Low Threshold. *Nano Lett*. 2021;21:1903–1914.
- [36] Harwell JR, Whitworth GL, Turnbull GA, et al. Green Perovskite Distributed Feedback Lasers. *Sci Rep*. 2017;7:1–8.
- [37] Srivastava AK, Zhang W, Schneider J, et al. Luminescent Down-Conversion Semiconductor Quantum Dots and Aligned Quantum Rods for Liquid Crystal Displays. *Adv Sci*. 2019;6:1901345.
- [38] Balmer RS, Brandon JR, Clewes SL, et al. Chemical vapour deposition synthetic diamond: Materials, technology and applications. *J Phys Condens Matter*. 2009;21.
- [39] Aharonovich I. Diamond nanocrystals for photonics and sensing. *Jpn J Appl Phys*. 2014;53:3–7.
- [40] Schirhagl R, Chang K, Loretz M, et al. Nitrogen-vacancy centers in diamond: Nanoscale sensors for physics and biology. *Annu Rev Phys Chem*. 2014;65:83–105.
- [41] Aharonovich I, Greentree AD, Prawer S. Diamond photonics. *Nat Photonics*. 2011;5:397–405.
- [42] Yu SJ, Kang MW, Chang HC, et al. Bright fluorescent nanodiamonds: No photobleaching and low cytotoxicity. *J Am Chem Soc*. 2005;127:17604–17605.
- [43] Wilson ER, Parker LM, Orth A, et al. The effect of particle size on nanodiamond fluorescence and colloidal properties in biological media. *Nanotechnology*. 2019;30.
- [44] Kumar R, Pandit P, Pal P, et al. Engineering bright fluorescent nitrogen-vacancy (NV) nano-diamonds: Role of low-energy ion-irradiation parameters. *AIP Adv*. 2018;8:085023.
- [45] Eggeling C, Widengren J, Rigler R, et al. Photobleaching of Fluorescent Dyes under Conditions Used for Single-Molecule Detection: Evidence of Two-Step Photolysis. *Anal Chem*. 1998;70:2651–2659.
- [46] Eggeling C, Widengren J, Rigler R, et al. Photostability of Fluorescent Dyes for Single-Molecule Spectroscopy: Mechanisms and Experimental Methods for Estimating Photobleaching in Aqueous Solution. *Appl Fluoresc Chem Biol Med*. Berlin: Springer; 1999. p. 193–240.
- [47] Kim JY, Voznyy O, Zhitomirsky D, et al. 25th anniversary article: Colloidal quantum dot materials and devices: A quarter-century of advances. *Adv Mater*. 2013;25:4986–5010.
- [48] Han KY, Willig KI, Rittweger E, et al. Three-dimensional stimulated emission depletion microscopy of

- nitrogen-vacancy centers in diamond using continuous-wave light. *Nano Lett.* 2009;9:3323–3329.
- [49] Torelli MD, Nunn NA, Shenderova OA. A Perspective on Fluorescent Nanodiamond Bioimaging. *Small.* 2019;15:1–20.
- [50] Reichwagen J, Hopf H, Del Guerzo A, et al. Photodimers of a soluble tetracene derivative. Excimer fluorescence from the head-to-head isomer. *Org Lett.* 2004;6:1899–1902.
- [51] Nair SR, Rogers LJ, Vidal X, et al. Amplification by stimulated emission of nitrogen- vacancy centres in a diamond-loaded fibre cavity. 2020;9:4505–4518.
- [52] Savvin A, Dormidonov A, Smetanina E, et al. NV– diamond laser. *Nat Commun.* 2021;12:1–8.

Graphical abstract

